Schutz (1998) and in Brady and Creighton (2000). The application of the Hough transform to periodic GWs is discussed in Krishnan *et al.* (2004). A search for periodic GWs from a single specific source, using the LIGO and GEO detectors, is described in Abbott *et al.* [LSC] (2004a). Limits on 28 isolated pulsar using the LIGO S2 run are given in Abbott *et al.* [LSC] (2005b).

- The importance of post-Newtonian corrections for the data analysis of coalescing binaries is emphasized in Cutler *et al.* (1993). Detailed discussions of data analysis procedure and parameter extraction for coalescences is given in Cutler and Flanagan (1994), Poisson and Will (1995), Królak, Kokkotas and Schäfer (1995) and Flanagan and Hughes (1998a). For computations of the waveform with the PN formalism, see the Further Reading section in Chapter 5.
- Optimal template placement for inspiraling compact binaries is discussed in Owen (1996) and Owen and Sathyaprakash (1999). A comparison of templates for binary inspiral is given in Damour, Iyer and Sathyaprakash (2001). A particularly useful family of templates for BH-BH inspiral have been proposed by Buonanno, Chen and Vallisneri (2003). A description of the LIGO search strategy for coalescences can be found in Abbott *et al.* [LSC] (2005a).
- The optimal SNR in a two-detector correlation and the overlap reduction function are discussed in Michelson (1987), Christensen (1992) and Flanagan (1993). A detailed discussion of signal processing strategies for stochastic backgrounds of GWs is given in Allen and Romano (1999). Signal chopping is discussed in Finn and Lazzarini (2001). Stochastic backgrounds of GWs are reviewed in Maggiore (2000). The search strategy of LIGO for stochastic backgrounds of GWs is discussed in Abbott *et al.* [LSC] (2004d) and (2005c).

Resonant-mass detectors

8

The history of experimental GW physics began with resonant-mass detectors. The pioneer was Joseph Weber who, in the 1960s, developed the concept and built the first resonant bars. In the course of the subsequent four decades, resonant-mass detectors operated by various groups have reached sensitivities better than Weber's original bars by about four orders of magnitudes in energy. Still, we will see in this chapter that these sensitivities could allow the detection of only relatively strong signals in our Galaxy or at most in our immediate galactic neighborhood, which are expected to be rare. To gain access to sources at large extragalactic distances it is necessary to build large interferometers, which will be the subject of the next chapter.

The passage from resonant detectors to interferometers implies a jump from "small-scale" experiments, performed by groups which can be as small as half a dozen people, to "Big Science", with collaborations of hundreds of people and financial costs which are higher by factors $O(10^2-10^3)$. As we will see in the next chapter, such a jump is justified by the formidable discovery potential of interferometers and especially advanced interferometers. We nevertheless begin our discussion of experiments with resonant-mass detectors, both because they still have the possibility of detecting rare or unexpected events, and also because their study is instructive in itself. Our emphasis will be on aspects that have an intrinsic conceptual interest, such as understanding how a GW interacts with a macroscopic piece of matter, and on how it is possible to detect vibrations of a macroscopic body which are incredibly small, with amplitude many orders of magnitude smaller than the size of a nucleus. We will see that, by themselves, resonant detectors are remarkable instruments; it is possible to measure vibrations in a two-ton object, such as a typical bar, which corresponds to just a few tens of phonons, and variations ΔL of their length L, with $\Delta L/L \sim 10^{-19}-10^{-18}$.

8.1 The interaction of GWs with an elastic body

8.1.1 The response to bursts

A typical bar is a cylinder of length $L \simeq 3$ m and radius $R \simeq 30$ cm, so in a first approximation we can treat its vibrations as one-dimensional. We orient the bar along the x axis, with the end-faces at $\pm L/2$, and we study the dynamics of a volume element dV of the bar originally located

at a position x. In the proper detector frame introduced in Section 1.3.3, under the action of the GW this volume element will be displaced to a new position $x+u(t,x)$, with $u(t,x) \ll x$. In this section we consider the response to a GW burst of duration τ_g much smaller than the relaxation time of the bar. As we will see in more detail later, for a typical bar this relaxation time is of order 600 s, and the approximation $\tau_g \ll 600$ s is excellent for astrophysical bursts, which can have $\tau_g = O(1)$ ms. In this case we can neglect dissipative effects in the bar during the passage of the burst, and we know from elasticity theory[1] that the longitudinal elastic oscillations of the material are governed by a wave equation,

$$dm \left(\frac{\partial^2 u}{\partial t^2} - v_s^2 \frac{\partial^2 u}{\partial x^2} \right) = dF_x(t,x) \,, \tag{8.1}$$

where dm is the mass of the volume dV considered, dF_x is the x component of the force exerted by the gravitational wave on the mass dm, and v_s is the speed of sound in the material, related to the Young modulus Y and to the density ρ by $v_s^2 = Y/\rho$.

[1] See, e.g. Landau and Lifshitz, Vol. VII (1970), or Love (1944).

Before proceeding with the formalism, we observe that eq. (8.1) is appropriate only if the effect of GWs on the bar can be approximated by a Newtonian force rather than by the full equations of general relativity. We saw in Chapter 1 that the effect of GWs on test masses can be approximated by a Newtonian force, and is expressed by the equation of the geodesic deviation (1.95), only if the spatial separation between test masses (and therefore, in our case, the size L of the bar) is much smaller than the typical scale of variation of the GWs, which in turn is equal to the reduced wavelength $\lambda\!\!\!^{-}$ of the waves. Otherwise, the expansion performed in the derivation of the equation of the geodesic deviation breaks down, and a full general relativistic treatment becomes necessary. As we will see in this chapter, the fundamental mode of the bar resonates at the frequency $\omega_0 = \pi v_s/L$, and the bar is sensitive to GWs with frequencies of the order of its resonance frequency. Then, the relation between the length L of the bar and the reduced wavelength $\lambda\!\!\!^{-}$ of the GW that it searches is $L/\lambda\!\!\!^{-} \simeq \pi v_s/c$. Of course, in any available material $v_s \ll c$. For instance, in aluminum at low temperatures, $v_s \simeq 5.4$ km/s and $\pi v_s/c \simeq 6 \times 10^{-5}$. Therefore for resonant bars the approximation $L/\lambda\!\!\!^{-} \ll 1$ is excellent and we can use the equation of the geodesic deviation to discuss their interaction with GWs.

Using eq. (1.95) we can write the Newtonian force in the proper detector frame in terms of the expression of h_{ij} in the TT frame,

$$dF_i = \frac{1}{2} \ddot{h}_{ij}^{TT} x^j \, dm \,, \tag{8.2}$$

with $x^j = (x+u, 0, 0)$. Since $u = O(h)$, to linear order in h we can simply set $x^j = (x,0,0)$ on the right-hand side of eq. (8.2). In this chapter the GW will always be expressed in the TT gauge and, to make the notation lighter, we omit the label TT from h_{ij}. Then we have $dF_x(t,z) = (1/2) x \ddot{h}_{xx} \, dm$, and eq. (8.1) becomes

$$\frac{\partial^2 u}{\partial t^2} - v_s^2 \frac{\partial^2 u}{\partial x^2} = \frac{1}{2} x \ddot{h}_{xx} \,. \tag{8.3}$$

The appropriate boundary conditions are

$$\left(\frac{\partial u}{\partial x} \right) \Big|_{x=\pm L/2} = 0 \,, \tag{8.4}$$

and express the fact that there is no flux of elastic energy flowing outside the bar. Equations (8.3) and (8.4) determine the elastic deformation of the bar produced by the GW. Again from elasticity theory we know that the energy stored in the elastic deformations is given by

$$E = \int dm \, \frac{1}{2} \left[\left(\frac{\partial u}{\partial t} \right)^2 + v_s^2 \left(\frac{\partial u}{\partial x} \right)^2 \right] . \tag{8.5}$$

The mode expansion compatible with the boundary conditions (8.4) is

$$u(t,x) = \sum_{n=0}^{\infty} \xi_n(t) \sin[\frac{\pi x}{L}(2n+1)] + \xi'_n(t) \cos[\frac{\pi x}{L}(2n+2)] \,. \tag{8.6}$$

Substituting into eq. (8.3) we get

$$\sum_{n=0}^{\infty} [\ddot{\xi}_n + \omega_n^2 \xi_n] \sin[\frac{\pi x}{L}(2n+1)] + [\ddot{\xi}'_n + {\omega'_n}^2 \xi'_n] \cos[\frac{\pi x}{L}(2n+2)] = \frac{1}{2} x \ddot{h}_{xx} \,, \tag{8.7}$$

with

$$\omega_n = \frac{\pi v_s}{L}(2n+1) \,, \qquad \omega'_n = \frac{\pi v_s}{L}(2n+2) \,. \tag{8.8}$$

Using the orthogonality relations

$$\int_{-L/2}^{L/2} dx \, \sin[\frac{\pi x}{L}(2n+1)] \sin[\frac{\pi x}{L}(2m+1)] = \frac{L}{2} \delta_{n,m} \,, \tag{8.9}$$

$$\int_{-L/2}^{L/2} dx \, \sin[\frac{\pi x}{L}(2n+1)] \cos[\frac{\pi x}{L}(2m+2)] = 0 \,, \tag{8.10}$$

we find from eq. (8.7)

$$\begin{aligned} \ddot{\xi}_n + \omega_n^2 \xi_n &= \frac{1}{L} \ddot{h}_{xx} \int_{-L/2}^{L/2} dx \, x \sin[\frac{\pi x}{L}(2n+1)] \\ &= \frac{(-1)^n}{(2n+1)^2} \, \frac{2L}{\pi^2} \ddot{h}_{xx} \,, \end{aligned} \tag{8.11}$$

while

$$\begin{aligned} \ddot{\xi}'_n + {\omega'_n}^2 \xi'_n &= \frac{1}{L} \ddot{h}_{xx} \int_{-L/2}^{L/2} dx \, x \cos[\frac{\pi x}{L}(2n+1)] \\ &= 0 \,. \end{aligned} \tag{8.12}$$

The latter integral vanishes because the integrand is odd under $x \to -x$, and therefore the modes ξ'_n do not couple to GWs.[2] We now restrict to the fundamental mode ξ_n with $n = 0$, whose dynamics is governed by the equation

$$\ddot{\xi}_0 + \omega_0^2 \xi_0 = \frac{2L}{\pi^2} \ddot{h}_{xx} \,, \tag{8.13}$$

[2] Physically this can be understood recalling, from Section 1.3.1, that the equation of the geodesic deviation describes displacements from a fixed point $x = 0$. Therefore, by definition, the volume element located at the origin does not move. In the case of a bar this means that, as long as we are interested only in its response to GWs, we can further impose the boundary condition $\xi(x=0,t) = 0$. The function $\sin[\pi x(2n+1)/L]$ satisfies it and therefore the modes $\xi_n(t)$ are allowed, while $\cos[\pi x(2n+2)/L]$ does not vanish at $x = 0$ and therefore $\xi'_n(t) = 0$. Of course, this result is specific to the form (8.2) of the force exerted by GWs. More specifically, it is a consequence of the spin-2 nature of the gravitational field, which is described by a traceless symmetric tensor with two indices $h_{ij}^{\rm TT}$, so to obtain dF_i we are forced to saturate one index with x^j.

with

$$\omega_0 = \frac{\pi v_s}{L} \,. \tag{8.14}$$

To obtain the elastic energy of this mode we replace $u(t,x)$ in eq. (8.5) with $\xi_0(t)\sin(\pi x/L)$. For a uniform bar of mass M we have $dm = (M/L)dx$, and we can perform the integral over x, obtaining

$$E = \frac{M}{4}(\dot\xi_0^2 + \omega_0^2\xi_0^2) \,. \tag{8.15}$$

Equations (8.13) and (8.15) show that the fundamental mode of a thin cylindrical bar of mass M and length L is formally identical to a harmonic oscillator with frequency ω_0 and mass $m_0 = M/2$, driven by a force $F(t) = (2/\pi^2)m_0 L\ddot h_{xx}$. Comparing with eq. (8.3), we see that this is the force exerted by GWs on a oscillator with an effective mass[3] m_0 and an effective length $l = (4/\pi^2)L$.

An oscillator of mass m_0 subject to an external impulsive force $F(t)$ absorbs from it an energy E_s (the label s stands for "signal") given by[4]

$$E_s = \frac{1}{2m_0}\left|\int_{-\infty}^{\infty} dt\, F(t)e^{-i\omega_0 t}\right|^2 \,. \tag{8.16}$$

The energy transferred to the fundamental mode of the bar by a GW burst is obtained using $F(t) = (2/\pi^2)m_0 L\ddot h_{xx}$ with $m_0 = M/2$, so

$$E_s = \frac{ML^2}{\pi^4}\left|\int_{-\infty}^{\infty} dt\, \ddot h_{xx}(t)\, e^{-i\omega_0 t}\right|^2 \,. \tag{8.17}$$

By definition, a burst is described by a function $h(t)$ which goes to zero very fast at $t \to \pm\infty$. We can therefore integrate by part twice the above expression, and we get

$$\begin{aligned} E_s &= \frac{ML^2(2\pi f_0)^4}{\pi^4}\left|\int_{-\infty}^{\infty} dt\, h_{xx}(t)e^{-i2\pi f_0 t}\right|^2 \\ &= 16ML^2 f_0^4\,|\tilde h_{xx}(f_0)|^2 \,. \end{aligned} \tag{8.18}$$

Therefore the value of $|\tilde h_{xx}(f_0)|^2$ can be obtained measuring the energy E_s deposited in the bar,[5]

$$\boxed{|\tilde h_{xx}(f_0)| = \frac{1}{4Lf_0^2}\sqrt{\frac{E_s}{M}} \,.} \tag{8.19}$$

It is interesting to see how an elastic bar, once excited by a GW, evolves in time. If we are interested in the long-time behavior of the signal, we must take into account that the energy E_s absorbed by the bar will be slowly dissipated by internal frictions. As we mentioned before, this dissipation takes place on a time-scale of about 600 s, which is much longer than the duration of a burst. Therefore, while the absorption of energy from a GW burst is extremely well described by eq. (8.13), to

[3] This value of the effective mass simply reflects the normalization of the normal modes. Here we have chosen $\sin[\pi x(2n+1)/L]$ as normal modes, which are normalized as in eq. (8.9). If we rather choose as normal modes $\Psi_n = \sqrt{2}\sin[\pi x(2n+1)/L]$ and we expand $u(x,t) = \sum_n a_n(t)\Psi_n(x)$, then $\xi_n(t) = \sqrt{2}\,a_n(t)$ and the effective mass of $a_n(t)$ is M rather than $M/2$. In Section 8.4, when we discuss resonant spheres, we will in fact adopt the latter normalization.

[4] See, e.g. Landau and Lifshitz, Vol. I (1976), eq. (22.12).

[5] Observe that this relation is completely independent of the shape of the burst, and E_s depends only on the Fourier component of the GW at the bar's resonance frequency f_0. This is a consequence of the fact that the duration of the burst τ_g is much smaller than the dissipation time so, as far as the absorption of energy from a burst is concerned, the resonance can be considered infinitely narrow.

study the subsequent time development of the signal we must generalize this equation to

$$\ddot\xi_0 + \gamma_0\dot\xi_0 + \omega_0^2\xi_0 = \frac{2L}{\pi^2}\ddot h_{xx} \,, \tag{8.20}$$

where γ_0 describes the effect of dissipation on the mode ξ_0. A very important parameter is the *quality factor* of the bar (or, more precisely, of the mode ξ_0) Q_0, defined by[6]

$$Q_0 = \frac{\omega_0}{\gamma_0} \,. \tag{8.21}$$

Experimentally, values of Q_0 of order 3×10^6 (and even up to 2×10^7) are obtained in bars at cryogenic temperatures, which corresponds, for $f_0 \sim 900$ Hz, to a relaxation time $1/\gamma_0 \sim 600$ s.

Equation (8.20) is easily solved going in Fourier space,

$$\tilde\xi_0(\omega) = T_0(\omega)\tilde h_{xx}(\omega) \,, \tag{8.22}$$

where[7]

$$T_0(\omega) = \frac{2L}{\pi^2}\,\frac{\omega^2}{\omega^2 - \omega_0^2 + i\gamma_0\omega} \tag{8.23}$$

is called the transfer function for the mode ξ_0. The form of $|T_0(\omega)|^2$ is shown in Fig. 8.1. We write $\omega^2 - \omega_0^2 + i\gamma_0\omega = (\omega - \bar\omega_+)(\omega - \bar\omega_-)$ with

$$\bar\omega_\pm = \pm\sqrt{\omega_0^2 - (\gamma_0/2)^2} - i\frac{\gamma_0}{2} \,. \tag{8.24}$$

In a typical bar γ_0 is smaller than ω_0 by a factor $Q_0 = O(10^6)$ so the second term in the square root is completely negligible and

$$\bar\omega_\pm \simeq \pm\omega_0 - i\frac{\gamma}{2} \,. \tag{8.25}$$

Then eq. (8.22) gives

$$\xi_0(t) = \frac{2L}{\pi^2}\int_{-\infty}^{\infty}\frac{d\omega}{2\pi}\,\frac{\omega^2\tilde h_{xx}(\omega)}{(\omega-\bar\omega_+)(\omega-\bar\omega_-)}\,e^{-i\omega t} \,. \tag{8.26}$$

As an example, we consider the case of a Dirac delta perturbation,

$$h_{xx}(t) = h_0\tau_g\,\delta(t) \,. \tag{8.27}$$

As discussed below eq. (7.99), this can be taken as a crude description of a burst of amplitude h_0 and duration τ_g. For the Dirac delta perturbation, the Fourier transform $\tilde h_{xx}(\omega) = h_0\tau_g$ is a constant and

$$\xi_0(t) = \frac{2L}{\pi^2}\,h_0\tau_g\int_{-\infty}^{\infty}\frac{d\omega}{2\pi}\,\frac{\omega^2}{(\omega-\bar\omega_+)(\omega-\bar\omega_-)}\,e^{-i\omega t} \,. \tag{8.28}$$

For $t<0$ we can close the contour in the upper half-plane and, since $\bar\omega_\pm$ both lies below the real axis, see eq. (8.24), we get zero, as required by causality. For $t>0$ we close the contour in the lower half-plane, where we pick the contribution of the two poles at $\omega = \bar\omega_\pm$, and we get

$$\xi_0(t) \simeq -\frac{2L}{\pi^2}\,h_0\omega_0\tau_g\,e^{-\gamma_0 t/2}\sin\omega_0 t \,. \tag{8.29}$$

We therefore have damped oscillations, and we see that, even if the GW burst lasts only a few ms, the bar continues to ring for a very long time, of order 10 min.

[6] In later sections we will meet other quality factors, like that of the transducer, or the total mechanical quality factor of the bar-transducer system. To avoid confusion, we denote by Q_0 (rather than simply by Q, as usually done in the literature) the quality factor of the mode ξ_0.

[7] The sign of the factor $i\gamma_0\omega$ depends on our conventions on the Fourier transform (see the Notation). Often in the literature the opposite convention on the Fourier transform is used, $F(t) = \int[d\omega/(2\pi)]\tilde F(\omega)e^{+i\omega t}$, and then $T_0(\omega) = (2L/\pi^2)\,\omega^2/(\omega^2 - \omega_0^2 - i\gamma_0\omega)$.

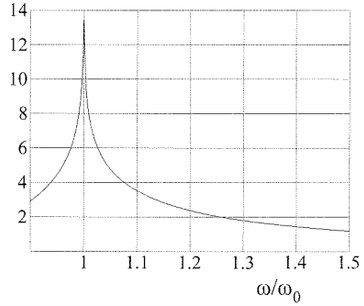

Fig. 8.1 The logarithm of the function $|(\pi^2/2L)T_0(\omega)|^2$, against ω/ω_0, for $Q_0 = 10^3$.

8.1.2 The response to periodic signals

We have seen that the fundamental mode of a resonant bar has an intrinsic time-scale $\tau_0 = 1/\gamma_0 \sim 10$ min, which is the time on which it dissipates its elastic energy due to internal frictions. GW bursts have a typical duration of the order of the ms, and therefore dissipation effects are completely negligible as long as we are interested in the total energy absorbed from the GW. For this reason, we could compute the energy absorbed by the bar during a burst setting $\gamma_0 = 0$, and the basic equation (8.19) is independent of γ_0.

For a periodic signal at the resonant frequency ω_0 the situation is different. Operatively, a periodic signal is just a wave-packet with frequencies around the resonant frequency ω_0 of the bar, sufficiently narrow in frequency space, so that its temporal duration is much longer than $1/\gamma_0 \simeq 10$ min. In the limiting case of an exactly monochromatic wave the temporal duration of the signal becomes infinite. If an ideal harmonic oscillator, with no losses, is driven by an exactly periodic force at its resonant frequency, its amplitude (and therefore the energy it absorbs) grows indefinitely. In a real harmonic oscillator there is a damping force proportional to $\gamma_0\dot{\xi}_0$ which becomes larger and larger as $\dot{\xi}_0$ grows, until the losses become so large that they compensate for the energy absorbed by the external source. At this point a stationary regime is reached.

To study the response of the fundamental mode of the bar to periodic signals we must therefore use eq. (8.20). We consider a wave propagating along the z axis,

$$h_{xx}(t) = h_0 \,\mathrm{Re}\left[e^{-i\omega(t-z/c)}\right] , \tag{8.30}$$

where h_0 is a real constant and Re denotes the real part. The bar is located in the plane $z = 0$, so

$$\ddot{\xi}_0 + \gamma_0\dot{\xi}_0 + \omega_0^2\xi_0 = -\frac{2Lh_0\omega^2}{\pi^2}\mathrm{Re}\left[e^{-i\omega t}\right] , \tag{8.31}$$

and a particular solution of this inhomogeneous equation is

$$\begin{aligned}\xi_0(t) &= \frac{2Lh_0\omega^2}{\pi^2}\,\mathrm{Re}\left[\frac{e^{-i\omega t}}{\omega^2-\omega_0^2+i\gamma_0\omega}\right] \\ &= \frac{2Lh_0\omega^2}{\pi^2}\,\frac{(\omega^2-\omega_0^2)\cos\omega t - \gamma_0\omega\sin\omega t}{(\omega^2-\omega_0^2)^2+\gamma_0^2\omega^2} .\end{aligned} \tag{8.32}$$

The energy of this solution is found from eq. (8.15). If $\omega = \omega_0$ it is time-independent, and is given by

$$\begin{aligned}E &= \frac{M}{4}(\dot{\xi}_0^2 + \omega_0^2\xi_0^2) \\ &= \frac{1}{\pi^4}ML^2h_0^2\omega_0^2Q_0^2 ,\end{aligned} \tag{8.33}$$

where $Q_0 = \omega_0/\gamma_0$. This shows that eq. (8.32) describes an equilibrium state where the energy absorbed by the wave is compensated by the losses due to friction. For an ideal oscillator, $Q_0 \to \infty$ and therefore $E \to \infty$. A bar which initially is not excited and which is then hit by a wave-packet centered around ω_0, with a spread of frequencies $\Delta\omega \ll \omega_0$, reaches asymptotically this solution after a transient time of order $1/\gamma_0$. At $\omega = \omega_0$ eq. (8.32) becomes

$$\xi_0(t) = -\frac{2L}{\pi^2}\,\frac{h_0\omega_0}{\gamma_0}\sin\omega_0 t . \tag{8.34}$$

Comparing this with the situation in which the bar is hit by a Dirac delta excitation, eq. (8.29) we see that, first of all, there is no exponential decay $\exp\{-\gamma_0 t/2\}$, since the periodic wave continuously feeds energy into the bar, compensating for the internal losses. And, second, the overall amplitude is much larger since $\tau_g \sim 1$ ms is now replaced by $1/\gamma_0 \sim 600$ s. Physically this is clearly understood: a burst excites the bar only for the short time τ_g, while under a periodic perturbation the amplitude of the oscillation keeps increasing for a time $1/\gamma_0$, until the rate of losses due to dissipation become equal to the rate at which energy is feed in by the GW, and an equilibrium regime is established.

8.1.3 The absorption cross-section

Equation (8.32) in principle characterizes completely the response of a bar to a monochromatic wave. However, it is instructive to express this result in terms of the cross-section of the bar for GW absorption.[8] The power absorbed by an oscillator with velocity $\dot{\xi}_0$ subject to a force $F(t)$ is $F(t)\dot{\xi}_0$. In our case, recalling that the effective mass of the mode ξ_0 is $M/2$, the force is

$$\begin{aligned}F &= \frac{M}{2}\,\frac{2L}{\pi^2}\ddot{h}_{xx} \\ &= -\frac{MLh_0\omega^2}{\pi^2}\cos\omega t ,\end{aligned} \tag{8.35}$$

and, using eq. (8.32),

$$F(t)\dot{\xi}_0 = 2M\left(\frac{Lh_0\omega^2}{\pi^2}\right)^2 \frac{\omega(\omega^2-\omega_0^2)\sin\omega t\cos\omega t + \gamma_0\omega^2\cos^2\omega t}{(\omega^2-\omega_0^2)^2+\gamma_0^2\omega^2} . \tag{8.36}$$

Since the energy of the incoming waves is defined as an average over several cycles, we are more interested in the average power absorbed over a cycle,

$$\begin{aligned}\frac{dE_{\rm abs}}{dt} &\equiv \langle F(t)\dot{\xi}_0\rangle \\ &= \frac{ML^2h_0^2}{\pi^4}\,\frac{\gamma_0\omega^6}{(\omega^2-\omega_0^2)^2+\gamma_0^2\omega^2} .\end{aligned} \tag{8.37}$$

In particular, at the resonance frequency

$$\frac{dE_{\rm abs}}{dt} = \frac{1}{\pi^4}ML^2h_0^2\omega_0^3Q_0 . \tag{8.38}$$

[8] We limit ourselves for the moment to a wave with pure + polarization, propagating in a direction perpendicular to the bar. See page 425 for the most general result.

Comparing with eq. (8.33) we see that at the resonant frequency (and once we have reached the stationary regime, where the solution for a bar initially at rest approaches (8.32)) $dE_{\rm abs}/dt = \gamma_0 E$. Of course $dE_{\rm abs}/dt$ depends both on the properties of the bar and on the intensity of the incoming radiation. A quantity that characterizes uniquely the detector is the *absorption cross-section* $\sigma_{\rm abs}(\omega)$, defined by

$$\frac{dE_{\rm abs}}{dt} = \sigma_{\rm abs}(\omega)\frac{dE_{\rm in}}{dAdt}\,, \tag{8.39}$$

where ω is the frequency of the incoming monochromatic wave and $E_{\rm in}$ is the incoming energy, so $dE_{\rm in}/dAdt$ is the energy arriving per unit time on a unit area, again averaged over a few cycles, as we always do for the energy of a wave. We consider a GW propagating along the z direction, with $h_+ = h_{xx} = h_0 \cos\omega t$ and $h_\times = 0$. Then, using eq. (1.155),

$$\frac{dE_{\rm in}}{dAdt} = \frac{c^3 h_0^2 \omega^2}{32\pi G}\,, \tag{8.40}$$

(where we used $\langle \cos^2 \omega t\rangle = 1/2$), and therefore

$$\sigma_{\rm abs}(\omega) = \frac{32\gamma_0 GML^2}{\pi^3 c^3}\,\frac{\omega^4}{(\omega^2-\omega_0^2)^2+\gamma_0^2\omega^2}\,. \tag{8.41}$$

[9] Numerically, setting $M = 2270$ kg, $L = 3$ m, $f_0 = 1$ kHz and $Q = 10^6$, we get $\sigma_{\rm abs}(\omega_0) \simeq 3\times 10^{-18}\,{\rm cm}^2$, which can be written as $\sigma_{\rm abs}(\omega_0) = \pi r^2$, with $r \simeq 10^{-9}$ cm. It is amusing to see that, even at the resonance, the cross-section for absorption of GWs of a whole two-ton bar is of order of the cross-section of a hard sphere (i.e. a sphere that absorbs with unit probability everything that arrives within its radius r) with a typical atomic size. This reflects of course the weakness of the gravitational interaction.

At the resonance frequency we have[9]

$$\sigma_{\rm abs}(\omega_0) = \frac{32GML^2\omega_0 Q_0}{\pi^3 c^3}\,. \tag{8.42}$$

The cross-section at resonance, however, is not really the best indicator of the detector sensitivity. Consider for instance a wave-packet whose Fourier modes $\tilde h(\omega)$ are approximately constant over a narrow interval $\omega_1 < \omega < \omega_2$ which includes the resonance frequency of the bar ω_0. The response of a bar to this wave-packet is determined by the integral of the cross-section

$$\int_{\omega_1}^{\omega_2} \frac{d\omega}{2\pi}\,\sigma(\omega)\,. \tag{8.43}$$

Since the cross-section is peaked around the resonance frequency ω_0, to compute this integral we can approximate $\sigma(\omega)$ using

$$\frac{\omega^4}{(\omega-\omega_0)^2(\omega+\omega_0)^2+\gamma_0^2\omega^2} \simeq \frac{\omega_0^2}{4(\omega-\omega_0)^2+\gamma_0^2}\,. \tag{8.44}$$

This approximation is the leading term in an expansion in $\gamma_0/\omega_0 = 1/Q_0$. Since $Q_0 \gg 1$, to a very good accuracy we have[10]

$$\int_{\omega_1}^{\omega_2} \frac{d\omega}{2\pi}\,\sigma(\omega) \simeq \frac{32\gamma_0 GML^2}{\pi^3 c^3}\int_{-\infty}^{\infty}\frac{d\omega}{2\pi}\,\frac{\omega_0^2}{4(\omega-\omega_0)^2+\gamma_0^2}\,. \tag{8.45}$$

Then, to leading order in $1/Q_0$, we find

$$\begin{aligned}\Sigma_0 &\equiv \int_{-\infty}^{\infty}\frac{d\omega}{2\pi}\,\sigma_{\rm abs}(\omega)\\ &= \frac{8GML^2\omega_0^2}{\pi^3 c^3}\,.\end{aligned} \tag{8.46}$$

[10] Observe that we extended the integral from $-\infty$ to $+\infty$. The error that we are introducing is negligible because the contribution to the integral from the region $|\omega-\omega_0| \gg \gamma_0$ is very small. For the same region, the detailed form of the incoming wave-packet is not important.

Using eq. (8.14) we can express ω_0 in terms of the speed of sound in the material, $\omega_0 = \pi v_s/L$, and then

$$\boxed{\Sigma_0 = \frac{8}{\pi}\,\frac{GM}{c}\,\left(\frac{v_s}{c}\right)^2\,.} \tag{8.47}$$

This shows that the result depends only on the mass M of the bar, and on the speed of sound in the material. Numerically, for an aluminum bar with mass $M = 2270$ kg, $\Sigma_0 \simeq 4.4\times 10^{-21}\,{\rm cm}^2\,{\rm Hz}$.[11]

Observe that the integrated cross-section is independent of Q_0, because the peak value of $\sigma(\omega)$ is proportional to Q_0, but such a large value is obtained only over a range $\Delta\omega \sim 1/Q_0$, so Q_0 cancels in $\int d\omega\,\sigma(\omega)$. More precisely, from the explicit expressions we see that the integrated cross-section is related to the cross-section at the peak by

$$\Sigma_0 = \frac{\gamma_0}{4}\,\sigma_{\rm abs}(\omega_0)\,. \tag{8.49}$$

Naively, one might then think that the value of Q_0 is not relevant for the performance of the detector. However, what really matters for detection is the ratio between the signal and the noise. In Section 8.3 we will discuss the possible sources of noise and we will appreciate the importance of having a large Q_0.

We will see below that, despite the fact that a resonant bar is a macroscopic object, weighting more than two tons, one is able to detect bar's oscillations which are so small that a classical treatment is no longer adequate, and it is instead appropriate to describe them in terms of the number of phonons that are excited.[12] It is therefore instructive to verify that the cross-section (8.46) is recovered in a quantum treatment of the fundamental mode ξ_0.

We have seen that the variable ξ_0 describes a harmonic oscillator of mass $m_0 = M/2$ and frequency ω_0. According to the standard rules of quantum mechanics, we promote it to an operator and we write

$$\xi_0 = \left(\frac{\hbar}{M\omega_0}\right)^{1/2}\left(a + a^\dagger\right)\,, \tag{8.50}$$

with $a, a^\dagger$ the creation and annihilation operators, and $[a, a^\dagger] = 1$ (compare with eqs. (8.171) and (8.172) below). The free Hamiltonian of the quantum oscillator is given by the familiar expression $H_0 = \hbar\omega_0(a^\dagger a + 1/2)$ and acts on the harmonic oscillator states labeled by $|n\rangle$. In a quantum field theory interpretation, the state vector $|n\rangle$ describes a collection of n phonons, each one with frequency ω_0. To compute the cross-section we study the interaction of this quantum harmonic oscillator with the classical external force given in eq. (8.35),[13]

$$F(t) = -(1/\pi^2)MLh_0\omega^2\cos\omega t\,. \tag{8.51}$$

We define the interaction Hamiltonian from $F = -\partial H_{\rm int}/\partial\xi_0$. In the quantum treatment the interaction Hamiltonian is then

$$H_{\rm int} = \frac{1}{\pi^2}\,MLh_0\omega^2\xi_0\cos\omega t$$

[11] Using eq. (8.11), it is straightforward to repeat the above computation for the n-th longitudinal mode ξ_n of the bar. Its resonance frequency is $\omega_n = (2n+1)\omega_0$, and for the cross-section, integrated around ω_n, we get

$$\Sigma_n = \frac{1}{(2n+1)^2}\,\Sigma_0\,. \tag{8.48}$$

Thus, the first excited mode of the bar which couples to GWs (ξ_n with $n = 1$) is at a frequency $f_1 = 3f_0$, and its integrated cross-section Σ_1 is smaller by a factor of 9 compared to the integrated cross-section Σ_0 of the fundamental mode.

[12] In particular, we will discuss in Sections 8.3.3 and 8.3.4 that the ultimate limitation of resonant bars, unless one uses quantum non-demolition techniques, is given by the so-called "standard quantum limit", where we are detecting single-phonon transitions induced by the GW.

[13] Any detectable GW is exceedingly classical, so we only need to use a quantum description for the oscillator.

$$= \frac{1}{\pi^2}(MLh_0\omega^2\cos\omega t)\left(\frac{\hbar}{M\omega_0}\right)^{1/2}\left(a+a^\dagger\right) . \qquad (8.52)$$

We assume that before the arrival of the GW the oscillator ξ_0 is in its ground state $|0\rangle$. To first order in perturbation theory, the interaction Hamiltonian (8.52) induces transitions to the state $|1\rangle$, with a transition amplitude

$$\begin{aligned} T_{0\to1} &= -\frac{i}{\hbar}\int_{-\infty}^{\infty} dt\, e^{-i\omega_0 t}\langle 1|H_{\rm int}|0\rangle \\ &= -i\frac{MLh_0\omega_0^2}{2\pi^2(\hbar M\omega_0)^{1/2}}\,2\pi\delta(\omega-\omega_0)\,, \end{aligned} \qquad (8.53)$$

where we have taken $\omega_0 > 0$, $\omega > 0$. The probability that a transition takes place at any time is $|T_{0\to1}|^2$. We regularize the time interval restricting to $-T/2 < t < T/2$, and therefore the transition rate is

$$\lim_{T\to\infty}\frac{1}{T}|T_{0\to1}|^2 = \frac{ML^2h_0^2\omega_0^3}{2\pi^3\hbar}\,\delta(\omega-\omega_0)\,, \qquad (8.54)$$

where we used the fact that, on a finite time interval $-T/2 < t < T/2$,

$$2\pi\delta(\omega) = \int_{-T/2}^{T/2} dt\, e^{i\omega T}\,, \qquad (8.55)$$

and therefore $2\pi\delta(\omega=0) = T$. In each transition is absorbed an energy $\hbar\omega_0$, therefore the energy absorbed per unit time is

$$\frac{dE_{\rm abs}}{dt} = \frac{ML^2h_0^2\omega_0^4}{2\pi^3}\,\delta(\omega-\omega_0)\,. \qquad (8.56)$$

The incoming flux corresponding to the force $F(t)$ is given by eq. (8.40). Using eq. (8.39), we then obtain

$$\sigma_{\rm abs} = \frac{32GML^2f_0^2}{\pi c^3}\,\delta(f-f_0)\,. \qquad (8.57)$$

Of course, having neglected the decay width of the excited quantum state, the cross-section is a Dirac delta rather than a curve with the Breit–Wigner shape (8.41). To compare with the classical calculation, it is simpler to consider the integral of $\sigma_{\rm abs}$ around the resonance, and from eq. (8.57) we get

$$\int df\,\sigma_{\rm abs} = \frac{32GML^2f_0^2}{\pi c^3}\,, \qquad (8.58)$$

in agreement with eq. (8.46). It is not difficult to check that the same result is obtained if the initial state of the oscillator is a generic state $|n\rangle$ rather than $|0\rangle$. (Observe that in this case the quantity relevant for the absorption of energy is $|T_{n\to n+1}|^2 - |T_{n\to n-1}|^2$).

Angular sensitivity and pattern functions

We have seen that the output of a resonant bar with its axis along the x direction is determined by the value of $h_{xx}(t)$. More generally, if we denote by $\hat{\mathbf{l}}$ the unit vector in the direction of the longitudinal axis of the bar, the scalar output is $h(t) = \hat{l}^i\hat{l}^j h_{ij}(t)$. Comparing with eq. (7.1) we see that the detector tensor of the bar is

$$D^{ij} = \hat{l}^i\hat{l}^j\,. \qquad (8.59)$$

Since h_{ij} is traceless, we can equivalently choose to define D^{ij} in the traceless form $D^{ij} = \hat{l}^i\hat{l}^j - (1/3)\delta^{ij}$. We now compute the pattern functions, defined in Section 7.1, for a cylindrical bar. The geometry is illustrated in Fig. 8.2. We denote by $\hat{\mathbf{n}}$ the unit vector in the propagation direction of the GW, with polar angles (θ,ϕ). We use as polar axis the longitudinal axis of the bar, so θ is the angle between $\hat{\mathbf{n}}$ and the x axis and, because of the cylindrical symmetry of the bar, we can take $\phi = 0$ without loss of generality. In Fig. 8.2, we have a reference frame (x,y,z), where the bar is along x axis and the y axis is perpendicular to the plane of the page, in the downward direction. Since we have set $\phi = 0$, the source is in the (x,z) plane. We introduce a second reference frame (x',y',z') such that the propagation direction $\hat{\mathbf{n}}$ of the GW coincides with the z' axis, and the y' axis is parallel to the y axis. Therefore the plane defined by the (x,z) axis is the same as the plane defined by the (x',z') axes (and is the plane of the page). The (x,z) axes are obtained from the (x',z') axis performing a counterclockwise rotation by an angle $\alpha = (\pi/2) - \theta$ around the y axis. In the (x',y',z') frame the GW has the form

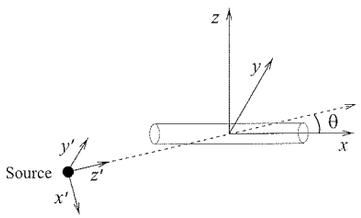

Fig. 8.2 The relation between the (x,y,z) and the (x',y',z') reference frames.

$$h'_{ij} = \begin{pmatrix} h_+ & h_\times & 0 \\ h_\times & -h_+ & 0 \\ 0 & 0 & 0 \end{pmatrix}_{ij}\,, \qquad (8.60)$$

where $h_{+,\times}$ are defined with respect to the (x',y') axes. To find the form of this GW in the (x,y,z) frame, we must compute how this tensor transforms under the rotation that brings the (x',y',z') frame onto the (x,y,z) frame. This rotation is described by the matrix

$$\mathcal{R} = \begin{pmatrix} \cos\alpha & 0 & \sin\alpha \\ 0 & 1 & 0 \\ -\sin\alpha & 0 & \cos\alpha \end{pmatrix}\,, \qquad (8.61)$$

with $\sin\alpha = \cos\theta$ and $\cos\alpha = \sin\theta$. The components of the tensor h_{ij} in the (x,y,z) frame are obtained from the components h'_{ij} in the (x',y',z') frame by $h_{ij} = \mathcal{R}_{ik}\mathcal{R}_{jl}h'_{kl}$. Then

$$\begin{aligned} h_{xx} &= \mathcal{R}_{1k}\mathcal{R}_{1l}h'_{kl} \\ &= h_+[(\mathcal{R}_{11})^2 - (\mathcal{R}_{12})^2] + 2h_\times\mathcal{R}_{11}\mathcal{R}_{12} \\ &= h_+\sin^2\theta\,. \end{aligned} \qquad (8.62)$$

Then we find $F_+(\hat{\mathbf{n}};\psi=0) = \sin^2\theta$ and $F_\times(\hat{\mathbf{n}};\psi=0) = 0$. The label $\psi = 0$ in $F_{+,\times}$ refers to the fact that these are the values of the pattern

functions when the plus and cross polarizations are defined with respect to the (x', y') axes. More generally, we might wish to refer the plus and cross polarizations to another system of axes, obtained rotating the (x', y') axes by an angle ψ around the z' axis.[14] We have already seen in eqs. (7.31) and (7.32) how F_+ and $F_\times$ transform under such a rotation, and then we get

$$h_{xx} = F_+(\hat{\mathbf{n}}; \psi) h_+ + F_\times(\hat{\mathbf{n}}; \psi) h_\times \,, \tag{8.63}$$

with

$$\boxed{F_+(\hat{\mathbf{n}}; \psi) = \sin^2\theta \, \cos 2\psi \,, \qquad F_\times(\hat{\mathbf{n}}; \psi) = \sin^2\theta \, \sin 2\psi \,.} \tag{8.64}$$

We see that the pattern functions have been determined by two factors: the geometry of the detector (which, in the case of resonant bars, is reflected in the fact that only the component h_{xx} enters, where x is the bar axis) and the transformation property of h_{ij} under rotations.

In general, we do not have experimental information on the polarization state of the wave, i.e. we do not know with respect to which axes the GW takes a given form. This could be the situation, for instance, when we search for GWs from a binary system of which we do not know the orientation of the orbit. In this case it can be useful to average $|\tilde{h}_{xx}(f)|^2$ over the angle ψ. We denote this average by $\langle \ldots \rangle_\psi$. Using eqs. (8.63) and (8.64) and the fact that $\langle \cos^2 2\psi \rangle_\psi = \langle \sin^2 2\psi \rangle_\psi = 1/2$ while $\langle \sin 2\psi \cos 2\psi \rangle_\psi = 0$ we get

$$\langle \, |\tilde{h}_{xx}(f)|^2 \, \rangle_\psi = \frac{1}{2} \sin^4\theta \left(|\tilde{h}_+(f)|^2 + |\tilde{h}_\times(f)|^2 \right) . \tag{8.65}$$

In eq. (8.47) we found the bar cross-section for a wave arriving from optimal direction, $\theta = \pi/2$, and a purely + polarization with optimal angle $\psi = 0$. We can now compute the bar cross-section for waves with arbitrary arrival direction. In the incoming energy, eq. (8.40), h_0^2 is replaced by $|h_+|^2 + |h_\times|^2$ (in eq. (8.40) we limited ourselves to the case $h_+ = h_0$, $h_\times = 0$) while, if we average over the polarization, from eq. (8.65) we find that in the absorbed energy h_0^2 is replaced by $(1/2)\sin^4\theta(|h_+|^2 + |h_\times|^2)$. Therefore the cross-section (8.47) is replaced by

$$\langle \Sigma_0(\theta) \rangle_\psi = \left(\frac{1}{2} \sin^4\theta \right) \frac{8}{\pi} \frac{GM}{c} \left(\frac{v_s}{c} \right)^2 . \tag{8.66}$$

The factor $\sin^4\theta$ is the price that we pay when the wave arrives from a non-optimal direction, while the factor $1/2$ reflects the fact that we are averaging over ψ rather than taking the optimal value. For GWs coming from all directions, a conventional measure of the sensitivity can be given by the average of this cross-section over the solid angle. Since the average of $\sin^4\theta$ over the solid angle is $8/15$, we find

$$\langle \Sigma_0(\theta) \rangle_{\psi,\theta} = \frac{32}{15\pi} \frac{GM}{c} \left(\frac{v_s}{c} \right)^2 . \tag{8.67}$$

[14] In general, a useful choice of axes, i.e. a preferred value of ψ, could be suggested by the geometry of the source. For instance, if the source is a binary star in an elliptic orbit, with the plane of the orbit perpendicular to the z' axis, a preferential frame will be given by the two major axes of the ellipse, and in this frame the GW amplitudes h_+ and $h_\times$ have a simpler form.

8.2 The read-out system: how to measure extremely small displacements

A resonant mass is a device that absorbs a very small fraction of the energy of the incoming GW and transforms it into mechanical oscillations. The next task is to detect these oscillations. It is here that most of the experimental ingenuity enters, and in fact the great improvements in the sensitivities of resonant bars from the times of Weber are due mostly to two factors: (1) The fact that bars have been cooled to cryogenic temperatures, as low as 0.1 K. (2) The continuous improvements in the read-out system.

To have a first idea of the difficulty of the problem, recall from eq. (8.29) that a GW burst with amplitude h_0, typical frequency f_0 and duration $\tau_g \sim 1/f_0$ drives oscillations of the fundamental mode of the bar with an amplitude $\xi_0 \sim L h_0$. From eqs. (7.109) and (7.112) we see that even a supernova explosion in our Galaxy, which is an event that takes place only a few times per century and, from numerical simulations, is expected to release 10^{-6}–10^{-7} solar masses in GWs in a few milliseconds, would produce on Earth a GW with at most $h_0 \sim 10^{-20}$. More realistically, to have some chances of detection we might need to reach a value $h_0 \sim 10^{-21}$. This gives

$$\xi_0 \sim 3 \times 10^{-21} \, \mathrm{m} \tag{8.68}$$

for a bar with $L \simeq 3$ m. This is a factor 10^6 smaller than the size of a nucleus, so such a measure might seem hopeless. As we will see in this and in the next section, this is not so, at least at a sensitivity level of $\xi_0 \sim 10^{-19}$–10^{-18} m, where resonant bars already perform routinely measurements. There are two main issues to address here. First, how it is possible to detect, in absolute terms, such a small displacement. This will be the subject of this section. The second issue is how to make sure that the effect of GWs is not swamped by much larger noise, and will be discussed in the next section.

Before entering into technical aspects, however, it is important to realize that what we want to measure is indeed an extremely small displacement, but it is a coherent displacement of a macroscopic body, such as the end-face of the bar, or the mirror of an interferometer. If we wanted to detect a displacement such as that given in eq. (8.68) on a microscopic scale, this would be utterly impossible. At the atomic scale, the notion of position of the bar end-point is not even defined with that precision. However, our sensors really detect the displacement of a macroscopic portion of the bar face (or of the mirror of an interferometer), and in this case the individual fluctuations at the microscopic level average out, and we are only left with the coherent part of the motion. It is intuitively clear, and we will see it quantitatively in the next section, that for instance thermal noise cannot easily generate collective vibrations of a very heavy object. The other important clue is that we do not really want to measure the displacement $\xi_0(t)$, but just some of

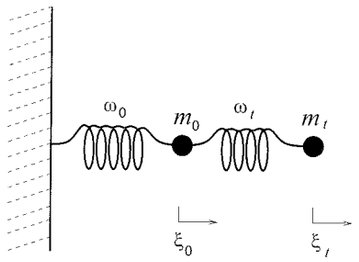

Fig. 8.3 The schematization of the bar–transducer system as a double oscillator.

its Fourier modes $\tilde{\xi}_0(f)$, in a frequency window where the effect of the GW is important. In this sense, eq. (8.68) is a bit misleading. The GWs that we are searching do indeed produce a displacement of this order in $\xi_0(t)$, but in Fourier space their contribution is localized in some frequency range, so we only have to fight against the Fourier modes of the noise in the same frequency range.

We now enter in the detail of how such a small displacement can be measured. In general, it is necessary to use a transducer, i.e. an object that transforms the displacement into an electric signal. A particularly convenient scheme is the *resonant transducer*. In a resonant transducer the displacement, before being converted into an electric signal, is amplified mechanically. This is obtained coupling the bar to an oscillator with a light mass. We will see in Section 8.2.2 how such a device is actually built, but for the moment we can simply schematize this system as a double oscillator, consisting of an oscillator with (effective) mass m_0 and frequency ω_0 coupled to an oscillator of (effective) mass m_t and frequency ω_t, as shown in Fig. 8.3. The first oscillator represents the fundamental mode of the bar, and we denote its displacement from the equilibrium position by $\xi_0(t)$. As we found in eq. (8.15), its effective mass m_0 is equal to $M/2$, where M is the mass of the bar. The second mass represents instead the transducer, and we denote its displacement from the equilibrium position by $\xi_t(t)$.[15]

8.2.1 The double oscillator

As a first step, we discuss the dynamics of the double oscillator. For the moment, we neglect dissipation effects. Then the system is described by the Lagrangian

$$L = \frac{1}{2} m_0 \dot{\xi}_0^2 + \frac{1}{2} m_t \dot{\xi}_t^2 - V(\xi_0, \xi_t)\,, \tag{8.70}$$

with

$$V(\xi_0, \xi_t) = \frac{1}{2} m_0 \omega_0^2 \xi_0^2 + \frac{1}{2} m_t \omega_t^2 (\xi_t - \xi_0)^2\,. \tag{8.71}$$

Defining $\mu = m_t/m_0$, the equations of motion in the presence of external forces F_0 and F_t acting on ξ_0 and ξ_t, respectively, are[16]

$$\ddot{\xi}_0 + \omega_0^2 \xi_0 + \mu \omega_t^2 (\xi_0 - \xi_t) = \frac{F_0}{m_0}\,, \tag{8.72}$$

$$\ddot{\xi}_t + \omega_t^2 (\xi_t - \xi_0) = \frac{F_t}{m_t}\,. \tag{8.73}$$

These equations are easily solved performing the Fourier transform and inverting the resulting 2×2 matrix. Consider in particular the response of the system to an impulsive force on the bar, like a GW burst, so that $F_0/m_0 = a_0 \delta(t)$, while we set $F_t = 0$, since the direct effect of the GWs on the light mass is much smaller than the "kick" that it receives from the bar, when the latter is hit by a GW. Then we get

$$\tilde{\xi}_0(\omega) = a_0 \, \frac{-\omega^2 + \omega_t^2}{(\omega^2 - \omega_+^2)(\omega^2 - \omega_-^2)}\,, \tag{8.74}$$

[15] In the pioneering times of Weber the transducer was a piezoelectric, i.e. a material (a ceramic or a crystal) that, under mechanical compression, becomes polarized and generates an electric field. So a piezoelectric is really sensitive to the strain $\partial\xi/\partial x$. For the mode ξ_n the spatial dependence is $\sin[\frac{\pi x}{L}(2n+1)]$ and

$$\frac{\partial}{\partial x} \sin[\frac{\pi x}{L}(2n+1)] \sim \cos[\frac{\pi x}{L}(2n+1)]\,. \tag{8.69}$$

Therefore the strain is maximum near the center of the bar, and the piezoelectrics were glued on the bar surface, near the midpoint. Modern resonant bars operate at low (2–4 K) or ultra-low (0.1–0.5 K) temperatures, both to reduce the thermal noise and to allow for the use of superconducting devices like SQUIDs in the read-out. Piezoelectrics, instead, are not suitable for cryogenic detectors, since some of their properties degrade at low temperatures; in particular, they have high intrinsic losses and therefore they lower the Q factor of the system. Piezoelectrics have therefore been abandoned, and all recent resonant-mass detectors have used the resonant transducer scheme.

[16] This schematization neglects back-action forces, that will be treated in Section 8.3.3. It also neglects the effect of the electric oscillator that performs the transduction process, see Section 8.2.2.

$$\tilde{\xi}_t(\omega) = a_0 \, \frac{\omega_t^2}{(\omega^2 - \omega_+^2)(\omega^2 - \omega_-^2)}\,, \tag{8.75}$$

where $\omega_\pm^2$ are the solutions of

$$\omega^4 - [\omega_0^2 + (1+\mu)\omega_t^2]\omega^2 + \omega_0^2 \omega_t^2 = 0\,. \tag{8.76}$$

We see that the bar-transducer system has two resonance frequencies $\omega_\pm$. Formally, at $\omega = \omega_\pm$, eqs. (8.74) and (8.75) state that $\tilde{\xi}_0(\omega)$ and $\tilde{\xi}_t(\omega)$ diverge. Once we include the dissipation terms in the equations, as we will do below, $\omega_\pm$ get an imaginary part and $\tilde{\xi}_0(\omega)$ and $\tilde{\xi}_t(\omega)$ at the resonances are large but finite. From eqs. (8.74) and (8.75) we get

$$\xi_0(t) = a_0 \int_{-\infty}^{\infty} \frac{d\omega}{2\pi} \, \frac{-\omega^2 + \omega_t^2}{(\omega^2 - \omega_+^2)(\omega^2 - \omega_-^2)} \, e^{-i\omega t}\,, \tag{8.77}$$

$$\xi_t(t) = a_0 \int_{-\infty}^{\infty} \frac{d\omega}{2\pi} \, \frac{\omega_t^2}{(\omega^2 - \omega_+^2)(\omega^2 - \omega_-^2)} \, e^{-i\omega t}\,. \tag{8.78}$$

Actually, these integrals are well defined only after we give a prescription for displacing the four poles (at $\omega = \pm\omega_+$ and at $\omega = \pm\omega_-$) from the real axis. In principle, we can find explicitly the imaginary parts of the poles including the dissipation terms in the equations, as indeed we will do below. However, this is not really necessary here, since the position of the poles with respect to the real axis is fixed by causality: $\xi_0(t)$ and $\xi_t(t)$ must both be zero at $t < 0$, i.e. before the Dirac delta perturbation arrives. Since for $t < 0$ we must close the contour in the upper half-plane, all poles must be in the lower half-plane, so that for $t < 0$ none of them contributes, and we correctly get $\xi_0(t) = 0$ and $\xi_t(t) = 0$. As a consequence, for $t > 0$, when we close the contour in the lower half-plane, we pick the contribution from all the four poles, which are circled clockwise. (We already checked explicitly this pole structure in the simpler case of eq. (8.28), see eq. (8.24).) Then a straightforward application of Cauchy theorem gives, for $t > 0$,

$$\xi_0(t) = \frac{a_0}{\omega_+^2 - \omega_-^2} \left(\frac{\omega_+^2 - \omega_t^2}{\omega_+} \sin\omega_+ t + \frac{\omega_t^2 - \omega_-^2}{\omega_-} \sin\omega_- t \right), \tag{8.79}$$

$$\xi_t(t) = \frac{a_0 \, \omega_t^2}{\omega_+^2 - \omega_-^2} \left(-\frac{1}{\omega_+} \sin\omega_+ t + \frac{1}{\omega_-} \sin\omega_- t \right). \tag{8.80}$$

Therefore the solution is a superposition of modes $\xi_\pm(t)$ oscillating with frequencies ω_+ and ω_-. Of course, $\xi_\pm(t)$ are simply the normal modes of the system, and the same results could have been found diagonalizing the Lagrangian.

We now consider the limit $\mu \ll 1$. In this case the amplitude of $\xi_t(t)$ is maximized taking $\omega_t = \omega_0$, apart from corrections of higher order in μ, This choice defines the *resonant* transducer. Then eq. (8.76) gives

$$\omega_\pm \simeq \omega_0 \left(1 \pm \frac{\sqrt{\mu}}{2} + O(\mu) \right), \tag{8.81}$$

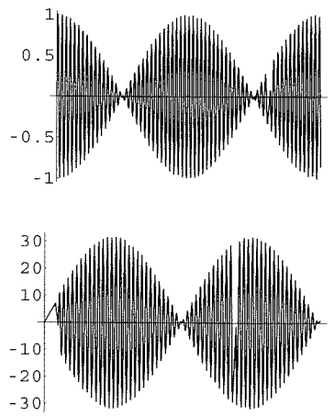

Fig. 8.4 The displacements of the bar, $\xi_0(t)$ (upper graph) and of the transducer, $\xi_t(t)$ (lower graph), both in units of a_0/ω_0, for $\mu = 10^{-3}$, as a function of $\omega_0 t$. Observe the difference in vertical scale between the two figures.

and the solutions (8.79) and (8.80) become

$$\xi_0(t) \simeq \frac{a_0}{2\omega_0}\left(\sin\omega_+ t + \sin\omega_- t\right) \tag{8.82}$$

$$\xi_t(t) \simeq \frac{a_0}{2\omega_0\sqrt{\mu}}\left(-\sin\omega_+ t + \sin\omega_- t\right) . \tag{8.83}$$

Writing $\omega_\pm = \omega_0 \pm \omega_b$, with $\omega_b = (1/2)\omega_0\sqrt{\mu} \ll \omega_0$, the above equations can be rewritten as

$$\xi_0(t) \simeq \frac{a_0}{\omega_0}\sin\omega_0 t\cos\omega_b t\,, \tag{8.84}$$

$$\xi_t(t) \simeq -\frac{a_0}{\omega_0\sqrt{\mu}}\cos\omega_0 t\sin\omega_b t\,, \tag{8.85}$$

so we have beatings between the two oscillators, and the energy flows periodically from the bar to the transducer and backward, with a frequency equal to the beat frequency ω_b, which is much smaller than ω_0. The evolution of the system is shown in Fig. 8.4.

The maximum oscillation amplitude of the transducer, A_t, is larger than the maximum oscillation amplitude of the bar, A_0, by a factor $1/\sqrt{\mu}$. This is the maximum value allowed by energy conservation, since it means that the elastic energy of the bar, $(1/2)m_0\omega_0^2A_0^2$, periodically is completely transferred to the transducer, so at that moment A_t is given by $(1/2)m_t\omega_0^2A_t^2 = (1/2)m_0\omega_0^2A_0^2$, and $A_t/A_0 = 1/\sqrt{\mu}$. We therefore have a mechanical amplification of the bar oscillation. This result suggests to take μ as small as possible. However, as we will see in Section 8.3, if we take m_t too small, the thermal noise of the transducer becomes large, and this fixes an optimal value of μ. The optimal values of μ is typically of order 10^{-3}–10^{-4}.

The conclusion is that, while the fundamental mode of the bar resonates at the frequency ω_0, the system composed by the bar's mode ξ_0 and the resonant transducer, with $\mu \ll 1$, has two resonant frequencies $\omega_\pm$, slightly displaced from ω_0 and given in eq. (8.81), and the oscillation amplitude of the transducer is larger than that of the bar's fundamental mode by a factor $1/\sqrt{\mu}$.

We now introduce dissipation in the system. Then eqs. (8.72) and (8.73) are replaced by

$$m_0[\ddot{\xi}_0 + \omega_0^2\xi_0 + \mu\omega_t^2(\xi_0 - \xi_t)] = F_0 + f_0^{\rm diss}\,, \tag{8.86}$$

$$m_t[\ddot{\xi}_t + \omega_t^2(\xi_t - \xi_0)] = F_t + f_t^{\rm diss}\,, \tag{8.87}$$

where, as before, F_0, F_t are the external forces. The dissipative forces $f_0^{\rm diss}, f_t^{\rm diss}$ are given by

$$f_0^{\rm diss} = -m_0\gamma_0\dot{\xi}_0 - m_t\gamma_t(\dot{\xi}_0 - \dot{\xi}_t)\,, \tag{8.88}$$

$$f_t^{\rm diss} = -m_t\gamma_t(\dot{\xi}_t - \dot{\xi}_0)\,, \tag{8.89}$$

where γ_0 and γ_t are related to the quality factors of the bar and of the transducer by $Q_0 = \omega_0/\gamma_0$ and $Q_t = \omega_t/\gamma_t$, respectively. Limiting

ourselves for simplicity to the lowest non-trivial order in $\mu = m_t/m$, we introduce the modes $\xi_\pm(t)$ from

$$\xi_0 = \frac{1}{\sqrt{2}}\left(\xi_+ + \xi_-\right), \qquad \xi_t = \frac{1}{\sqrt{2\mu}}\left(-\xi_+ + \xi_-\right). \tag{8.90}$$

In terms of $\xi_\pm(t)$ the equations of motion, with the inclusion of the dissipative terms, become

$$\ddot{\xi}_+ + \bar{\gamma}\,\dot{\xi}_+ + \frac{\gamma_0 - \gamma_t}{2}\dot{\xi}_- + \omega_+^2\xi_+ = \frac{1}{\sqrt{2}}\left(\frac{F_0}{m_0} - \sqrt{\mu}\frac{F_t}{m_t}\right), \tag{8.91}$$

$$\ddot{\xi}_- + \bar{\gamma}\,\dot{\xi}_- + \frac{\gamma_0 - \gamma_t}{2}\dot{\xi}_+ + \omega_-^2\xi_- = \frac{1}{\sqrt{2}}\left(\frac{F_0}{m_0} + \sqrt{\mu}\frac{F_t}{m_t}\right), \tag{8.92}$$

where $\omega_\pm^2 = \omega_0^2(1 \pm \sqrt{\mu})$ and $\bar{\gamma} = (\gamma_0 + \gamma_t)/2$. We see that these equation decouple only if $\gamma_0 = \gamma_t$ (and in this case, as well as in the absence of dissipation, $\xi_\pm(t)$ are the two normal modes of the system). Going in Fourier space, it is easy to find the solution for $\tilde{\xi}_\pm$ and therefore for $\tilde{\xi}_t$, which is[17]

$$\boxed{\tilde{\xi}_t(\omega) = \frac{(\tilde{F}_0(\omega)/m_0)\omega_0^2 - (\tilde{F}_t(\omega)/m_t)(\omega^2 - \omega_0^2 + i\omega\gamma_0)}{(\omega^2 - \omega_+^2 + i\omega\bar{\gamma})(\omega^2 - \omega_-^2 + i\omega\bar{\gamma})}\,.} \tag{8.93}$$

[17] In the denominator we neglected a term that depends on $(\gamma_t - \gamma_0)^2\omega^2$ and, numerically, is totally negligible.

This general result will be useful in Section 8.3 when we study the different sources of noise acting on the bar and on the transducer. For the moment we are only interested in the response to a GW so we set, according to eq. (8.13) $\tilde{F}_0(\omega) = -(2L/\pi^2)m_0\omega^2\tilde{h}(\omega)$, and $\tilde{F}_t(\omega) = 0$. Then we find

$$\tilde{\xi}_t(\omega) = T_t(\omega)\tilde{h}(\omega)\,, \tag{8.94}$$

where the transducer transfer function is

$$\boxed{T_t(\omega) = -\frac{2L}{\pi^2}\,\frac{\omega_0^2\omega^2}{(\omega^2 - \omega_+^2 + i\omega\bar{\gamma})(\omega^2 - \omega_-^2 + i\omega\bar{\gamma})}\,.} \tag{8.95}$$

The squared modulus of this transfer function is shown in Fig. 8.5 (solid line), together with the the same quantity for a single oscillator (dashed line), given in eq. (8.23) and already shown in Fig. 8.1. Observe that, because of the small value of μ, the two peak values of the transducer transfer function are much larger than the peak value of a bar alone, having the same quality factor. In contrast, at $\omega \gg \omega_0$ $|T_t(\omega)|$ goes to zero as $1/\omega^2$, while $|T_0(\omega)|$ goes to a constant.

We see that dissipation is governed by $\bar{\gamma}$. We can then define the mechanical quality factor of the bar-transducer system by $\bar{\gamma} = \omega_0/Q_m$, i.e.

$$\frac{1}{Q_m} = \frac{1}{2}\left(\frac{1}{Q_0} + \frac{1}{Q_t}\right). \tag{8.96}$$

Typical values that have been reached in resonant bars are of order $Q_m \sim 10^6$.

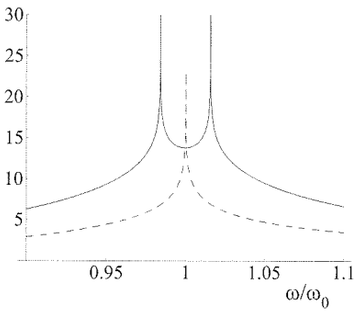

Fig. 8.5 $\mathrm{Log}_{10}|(\pi^2/2L)T_t(\omega)|^2$ as a function of ω/ω_0, for $\bar{Q} = \omega_0/\bar{\gamma} = 10^6$ and $\mu = 10^{-3}$ (solid line) and the same quantity for the bar alone, with $Q = 10^6$ (dashed line), plotted against ω/ω_0.

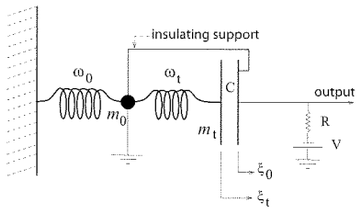

Fig. 8.6 A schematic representation of the capacitive transducer.

[18]Observe that, in these schemes, the quantity that is actually monitored is not ξ_t but $\xi_t - \xi_0$. The transfer function for $\xi_t - \xi_0$ is easily obtained repeating the steps that led to eq. (8.95). However, by construction the amplitude of ξ_t is much larger than the amplitude of ξ_0, so $\xi_t(t) - \xi_0(t) \simeq \xi_t(t)$.

8.2.2 Resonant transducers

The double oscillator provides a mechanical amplification of the oscillation of the bar. The next step is to read the displacement of the light mass, transforming it into in an electric signal. Various schemes have been devised by different experimental groups. The principle of all these transducers is to use the displacement of the small mass to modulate a stored electromagnetic field. In general terms, transducers can be distinguished between passive and active (also called parametric). Passive transducers modulate a d.c. field, while parametric transducers modulates an a.c. field generated by an external source.

In particular, in capacitive transducers a d.c. electric field is stored in the gap of a capacitor (values of the gap as small as 10 μm have been obtained). The light mass of the double oscillator is used as one of the plate of the capacitor, while the other plate is rigidly fixed with an electrically isolated support to the bar face so, in the same schematization used in the previous section for the double oscillator, the system is as shown in Fig. 8.6. In inductive transducers, instead, a persistent superconductive current is stored in a flat coil. The light mass of the double oscillator is now a superconductive ground plane, whose oscillations induce modulations of the inductance.[18]

The resulting electric signal is still very small and must be further amplified electronically. At cryogenic temperatures the best amplifier is invariably a SQUID. However, here we face a problem of mismatch between the large output impedance of the transducer, $1/(\omega C) \sim 10^5$ ohm, and the small input impedance of the SQUID, $\omega L_{\rm SQ} \sim 10^{-2}$ ohm. Optimal signal transfer is then obtained inserting a transformer between the transducer and the SQUID. As a result, we end up with a system of three oscillators, two mechanical (the oscillation ξ_0 of the bar and the oscillation ξ_t of the transducer) and one electric (the LC circuit formed by the transducer capacitance and the transformer inductance). These oscillators are coupled, and therefore the system is described by a generalization of eqs. (8.86) and (8.87) that includes the dynamics of the electric mode. The full system of equations is somewhat complicated. However, to get a qualitative understanding, we observe that the strength of the coupling between oscillators can be measured by the fraction of the energy that flows from one to the next. For the two mechanical oscillators we have seen that, taking $\mu \ll 1$ and tuning $\omega_t = \omega_0$, all the energy of the first oscillator (the bar) can be transferred periodically to the second (the transducer), with a beating frequency $\omega_b = \omega_0\sqrt{\mu}$. We want to characterize similarly the coupling between the transducer and the electric mode.

For this, we start by observing that the output of the electromechanical transducer is a potential V, which is a linear function of the transducer motion, so a displacement $\tilde{\xi}_{\rm t}$ of the transducer generates a potential V given, in Fourier transform, by

$$\tilde{V}(\omega) = \alpha(\omega)\tilde{\xi}_{\rm t}(\omega)\,. \tag{8.97}$$

When $\alpha(\omega)$ is a constant, the potential $V(t)$ is linear in $\xi_{\rm t}(t)$ while, if $\alpha(\omega) \sim i\omega$, the potential $V(t)$ is linear in $d\xi_{\rm t}(t)/dt$. On the relatively small frequency range of interest for resonant bars, α can usually be approximated by its value at ω_0, which means that we can write eq. (8.97) equivalently as $V(t) = \alpha\,\xi_{\rm t}(t)$, or as

$$V(t) = Z_{21}\dot{\xi}_{\rm t}(t)\,, \tag{8.98}$$

with $Z_{21} = \alpha/(-i\omega_0)$. The electromagnetic energy $E_{\rm em} = (1/2)CV^2$ of the capacitive transducer is then given by

$$E_{\rm em} = \frac{1}{2}C\alpha^2\xi_{\rm t}^2\,. \tag{8.99}$$

The elastic energy of a transducer is[19]

$$E_{\rm elas} = \frac{1}{2}m_{\rm t}\omega_0^2\xi_{\rm t}^2\,. \tag{8.100}$$

The ratio of these energies, β, gives a measure of the transfer of energy from the bar to the electric mode,

$$\beta \equiv \frac{E_{\rm em}}{E_{\rm elas}} = \frac{C\alpha^2}{m_{\rm t}\omega_0^2} = \frac{\alpha^2}{m_{\rm t}\omega_0^3|Z|}\,, \tag{8.101}$$

where $|Z| = 1/\omega_0 C$ is the impedance. Recalling the definition $Z_{21} = \alpha/(-i\omega_0)$ we can also write

$$\beta = \frac{|Z_{21}|^2}{m_{\rm t}\omega_0|Z|}\,. \tag{8.102}$$

Observe that β is inversely proportional to the mass of the transducer $m_{\rm t}$. If, instead of using the resonant transducer scheme, one coupled directly the bar to the capacitor, β would rather be proportional to $1/m_0$, where m_0 is the effective bar mass, and the transfer of energy from the bar to the amplifier would be much less effective. Thus, we can see the resonant transducer as the solution to a problem of impedance matching: the mechanical output impedance of the bar is very high, compared to the mechanical impedance of the electric field in the capacitor, and the light mass in the resonant transducer scheme plays the role of a mechanical transformer for the bar elastic energy.

The best coupling between the mechanical modes and the electric mode is obtained setting $\omega_{\rm em} = \omega_0$, in which case the two mechanical modes and the electric mode are all in resonance. Unfortunately, to obtain a high quality factor for an electric circuit is more difficult than for mechanical resonators. If we couple resonantly our double oscillator with a mechanical quality factor $Q_m \sim 10^6$ to an resonant electric circuit with a quality factor $Q_{\rm em}$ much lower than 10^6, in the electro-mechanical system composed by the two mechanical oscillators and the electric circuit, dissipation would take place mostly when the energy is in the electric circuit. As we will discuss in Section 8.3.1, a high overall Q is however necessary in order to fight thermal noise. One solution, which has been

[19]More precisely, since the transducer is an extended object, the relation between $E_{\rm elas}$ and $\omega_0^2\xi_{\rm t}^2$ includes numerical factors of order one that depends on the geometry of the transducer, and $m_{\rm t}$ is an effective mass, defined so that eq. (8.100) holds, and which differ from the actual transducer mass by a factor of order one.

used by all detectors until recently, is to detune the electric mode, keeping its frequency $f_{\rm em}$ about 30% higher than the resonances of the two mechanical modes because, if the oscillators are detuned, only a fraction of the total energy $O(\beta)$ is transferred to the electric mode, where it is dissipated fast. The drawback of this solution is that the bandwidth of the detector increases with β, so a small β means a narrow bandwidth.[20]

However, recently various groups have improved the quality factor of the electric resonator and brought it in resonance, or close to the mechanical modes. As a result, the bandwidth of the detectors has been greatly enhanced, and in particular for the AURIGA detector is now of order or larger than 100 Hz, see Fig. 8.17 below.

We have now transformed the bar displacement into an electromagnetic signal, and the final step of the transduction process is its amplification. At cryogenic temperatures, SQUIDs are by far the amplifiers with the lowest noise, so they are the natural choice for the final amplification chain in resonant detectors.[21] In this way it has been possible to measure changes in energy corresponding to the absorption of $O(100)$ quanta of frequencies ω_0, i.e. $\Delta E = N\hbar\omega_0$ with $N = O(100)$. This is quite remarkable, if we think that we are detecting vibrations corresponding to just about 100 phonons, in a two-ton object!

Alternative read-out systems have also been actively investigated. We briefly discuss two possibilities.

Parametric resonant transducers

These transducers make use of an external power source (the "pump" oscillator). The oscillation of the light mass in the double oscillator can be used to modulate a capacitance, just as in the capacitive transducer discussed above, but the capacitor is now part of a high-Q resonant circuit which, in turn, modulates the phase and amplitude of the reflected or transmitted signal. This produces sidebands at the frequencies $\omega_{\rm p} \pm \omega_0$, where $\omega_{\rm p}$ is the pump frequency, which can be at optical, microwaves or radio frequencies. Then the signal is demodulated using as reference the original pump signal. Contrary to passive devices, parametric transducers have an intrinsic power gain, due to the up-conversion of the signal to much higher frequencies. We can see passive transducers as objects in which the transduction process, i.e. the transformation of the mechanical oscillations into an electric signal, is completely separated by the amplification process, which is performed later by a SQUID. In parametric devices, instead, the transduction and at least part of the amplification are performed simultaneously. On the other hand, for parametric transducers, important limitations come from phase noise and stability problems in the pump. It is also necessary an excellent carrier suppression, otherwise the pump power reflected from the cavity overwhelms the signal in the sidebands.

An important difference between passive and parametric transducers is that in passive transducers the relation between the input and the output is linear, both in amplitude and in phase, while this is not the

[20] We will see this formally in Section 8.3.2, see in particular Note 27. However, the reason can be understood physically observing that, if β is small, only a small part of the total energy flows from the mechanical modes to the electric mode, so the oscillation amplitude of the electric mode is small. To pick up a signal with a smaller oscillation amplitude we need a larger integration time, and a large integration time means a small bandwidth, $\Delta f \sim 1/\Delta t$. Furthermore, with a larger value of β, a smaller mechanical amplification is required, and the mass $m_{\rm t}$ of the resonant transducer can be made heavier. As we will see in Section 8.3.1, this reduces the transducer thermal noise, which is another fact that limits the bandwidth.

[21] Actually, both the AURIGA and MiniGRAIL groups developed double-stage SQUIDS, in which a dc SQUIDs senses the signal and its output is further amplified by a second stage SQUID.

case for a parametric transducer, because of the effect of the external pump field. We will see in Section 8.3.3 that, because of the role of the uncertainty principle in the measurement process, this difference has important implications for the ultimate sensitivity attainable with passive and with parametric transducers.

Dual detectors

The resonant transducer scheme has two advantages. The first is that it provides a much needed mechanical amplification of the signal. The second is that, since it amplifies only the mode to which it is tuned (normally the fundamental mode of the bar) it allows us to forget about all the higher modes of the bar. This means that we can neglect the thermal noise associated to all the higher modes ξ_n of the bar, and we can describe the bar–transducer system as a simple system with two degrees of freedom, ξ_0 and ξ_t.

On the other hand, when in the next section we discuss the various contributions to the noise, we will see that the resonant transducer also introduces an important limitation. In particular, because of its thermal noise the sensitivity of a resonant bar is restricted to a relatively narrow region Δf around its resonance frequency.

An alternative that has been recently proposed is the so-called *dual resonator*. In this scheme one has two nested objects, such as two concentric cylinders, or an outer hollow sphere and an inner concentric solid sphere. One can arrange the size and material so that the fundamental mode of the inner body $f_{\rm inner}$ is, say, around 3 kHz, while the fundamental mode of the outer body, $f_{\rm outer}$ is around 1 kHz. The idea is to measure the differential displacement between these two surfaces. The displacement could for instance be detected by an optical read-out made of a high-finesse Fabry–Perot cavity,[22] resonant with an incident laser beam, as in Fig. 8.7. Since no resonant transducer is introduced, the useful bandwidth covers the whole interval $f \in [f_{\rm outer}, f_{\rm inner}]$ (in fact, in this region one can even show that the oscillation amplitude of the two nested bodies adds up, while some noise partially cancel).

The first problem that must be solved is to have sufficient power in the cavity and a sufficiently high finesse, in order to be able to reach the required sensitivity, taking into account that we have given up the amplification that was provided by the resonant transducer scheme. Cavities of this type are being developed, but still we are not yet at the required sensitivity level. Second, one should find a way to get rid of the contribution of all the higher modes. In the resonant transducer scheme one has a selective read-out based on frequency: only the mode with the same frequency as the resonant transducer is amplified. In the dual scheme, it has been proposed a geometrically based mode selection, which consists in sensing a large portion of the surface, so that the effect of higher modes averages out and, comparing the deformations on different parts of the body, one can enhance the contribution of deformations with a quadrupolar symmetry.

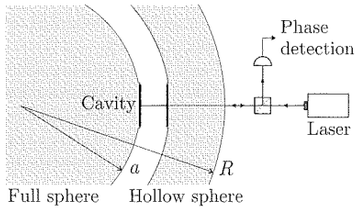

Fig. 8.7 Scheme for a possible read-out of a dual detector. The small gap between the two spheres is measured using a high-finesse single-ended cavity. Reprinted figure with permission, from Briant *et al. Phys. Rev. D* **67**, 102005 (2003). Copyright 2003 by the American Physical Society.

[22] Fabry–Perot cavities will be discussed in detail when we come to interferometers, in Chapter 9.

8.3 Noise sources

In this section we examine the sources of noise that limit the performances of resonant bars. In particular, in Sections 8.3.1 and 8.3.2 we discuss the two types of noise that are more important in existing detectors, namely thermal noise and read-out noise, and we will see that their combination fixes the useful frequency bandwidth. We will then discuss other sources of noise, including some fundamental limitations imposed by quantum mechanics.

For each source of noise, we can characterize its effect in two complementary ways: (1) We can compute the minimum detectable energy that should be deposited in a bar by a short GW burst in order to overcome this noise, say at signal-to-noise ratio $S/N = 1$. (2) We can give its contribution to the noise spectral density. The former characterization is physically more intuitive, but it carries less detailed information, because it is a quantity integrated over the frequency bandwidth. The noise spectral density, on the other hand, carries the full spectral information. Below we will use both characterizations.

The noise spectral density has been defined in Section 7.1. To compute it, for resonant bars it is convenient to proceed as follows. First of all, we write as usual the output of the detector in the form $s(t) = h(t) + n(t)$, where $h(t)$ is the contribution due to GWs and $n(t)$ is the noise.[23] We have seen that, when GWs provide the only force acting on the bar, the corresponding displacement, that we denote here by $\xi^{(h)}$ is related to the GW by

$$\tilde{\xi}^{(h)}(\omega) = T(\omega)\tilde{h}(\omega)\,, \tag{8.103}$$

where $T(\omega)$ is the transfer function. We can use this equation to study the displacement of a single oscillator like the bar fundamental mode ξ_0, in which case the transfer function is the function $T_0(\omega)$ given in eq. (8.23), or we can use it to study the transducer displacement ξ_t, in which case the transfer function is given in eq. (8.95). The latter quantity is more relevant, since it is the motion of the transducer that is sensed, but it can also be useful to compare the situation with the resonant transducer with what happens if we have only the mode ξ_0.[24] We denote generically by ξ the displacement in which we are interested, either ξ_0 or ξ_t, and it is understood that the corresponding transfer function is used.

The noise gives further contributions to the displacement,

$$\tilde{\xi}^{(n)}(\omega) = T(\omega)\tilde{n}(\omega)\,. \tag{8.104}$$

Following the general definition of spectral density given in Section 7.1, the single-sided spectral density of a displacement, $S_\xi(\omega)$, is defined by

$$\langle \xi^2(t)\rangle = \int_0^\infty \frac{d\omega}{2\pi}\, S_\xi(\omega)\,, \tag{8.105}$$

Using eq. (8.104) we see that the noise spectral density $S_n(\omega)$ is related to the spectral density of the displacement induced by that noise by

$$S_\xi^{\rm noise}(\omega) = |T(\omega)|^2\, S_n(\omega)\,. \tag{8.106}$$

[23] More precisely, $n(t)$ is the noise referred to the detector's input, see the discussion in Section 7.1.

[24] Observe that the use of the transfer function of the bar–transducer system is still an oversimplification. We have seen that the electromagnetic transducer is really a three-mode system composed by the bar, transducer, and electric mode. If the electric mode is detuned, a two-mode description can be sufficient. Otherwise, the full transfer function of the three-mode system must be used for a detailed quantitative understanding. Thus, the analysis that we present below is really meant to obtain only a qualitative understanding of the effect of the principal noise in a resonant detector, and is not sufficient to reproduce accurately the details of the sensitivity curves.

Therefore, to compute the contribution to $S_n(\omega)$ due to a given noise source, say thermal noise, we can compute the spectral density of the displacement induced by this noise, and we then divide it by $|T(\omega)|^2$.[25]

8.3.1 Thermal noise

Thermal (or Brownian) noise is due to the thermal kinetic energy of the atoms of the detector. Naively one might think that, in a bar at temperature T, the minimum detectable energy excitation should be $\Delta E_{\rm min} \simeq kT$, otherwise the excitation is drown into the thermal fluctuations. A key contribution by Weber was the realization that, in a mechanical oscillator with a high Q, the minimum detectable energy due to thermal noise is in fact much smaller. The physical intuition behind this result is that a high-Q oscillator dissipates very slowly; if we excite the oscillator, we know that it will return to its original state in a very long time. In particular, the fundamental mode of a bar has a relaxation time $\tau_0 = 1/\gamma_0 = Q_0/\omega_0$ of order 10 min, which means that it is extremely weakly coupled to the thermal bath constituted by all other bar's modes. Therefore we expect not only that the time needed to go from an excited state back to the ground state will be long but also, conversely, that the time needed to develop energy fluctuations of order kT in the fundamental mode will be of order τ_0.

On the other hand we have seen that a GW burst, in a time τ_g corresponding to the burst duration, excites bar's oscillations with an amplitude $\xi_0 \sim hL$. Since τ_g is much smaller than the relaxation time τ_0 of the fundamental mode of the bar, we can expect that the energy fluctuations due to thermal noise in such a short time are much smaller than kT, and rather of order $kT\,(\tau_g/\tau_0)$. The idea is therefore that, if we sample the bar's state with a time resolution Δt, the minimum GW energy detectable against thermal noise should be

$$\boxed{(\Delta E_{\rm min})_{\rm thermal} \simeq kT\,\frac{\Delta t}{\tau_0}\,,} \tag{8.107}$$

as long as $\Delta t \geqslant \tau_g$ (of course, if Δt become smaller than the burst duration, we start to lose part of the signal). In practice this will be achieved using the matched filtering procedure of Section 7.3, with a filter functions, such as a Dirac delta, that discriminates a fast excitation from the slow thermal modes.

To confirm this physical intuition, we study the evolution of the bar's fundamental mode in the presence of thermal noise. In the previous sections we studied the evolution of ξ_0 using the equation for the damped oscillator,

$$\ddot{\xi}_0 + \omega_0^2\xi_0 = -\gamma_0\dot{\xi}_0\,. \tag{8.108}$$

If this were the complete description of the bar's dynamics, the time evolution of $\xi_0(t)$ would be fully deterministic. In principle, we could then simply subtract it, and attribute any deviation from the expected evolution to external causes like GWs. However, thermal noise enters in

[25] Observe that $S_n(\omega)$ has dimensions Hz^{-1}, so the strain sensitivity $S_n^{1/2}(\omega)$ has dimensions $\mathrm{Hz}^{-1/2}$, while $S_\xi(\omega)$ has dimensions m^2/Hz. The sensitivity of the bar is usually displayed plotting either $S_n(\omega)$ or $S_n^{1/2}(\omega)$. This is more useful than plotting $S_\xi(\omega)$ or $S_\xi^{1/2}(\omega)$, especially when we compare the sensitivity of different experiments like bars and interferometers. In fact, a bar and an interferometer with the same sensitivity to GWs, i.e. with the same $S_n(\omega)$, would have very different spectral density of the displacement, since for bars the length-scale that enters in the transfer function is the bar's length $L = 3$ m, while for interferometers it is the pathlength of the light in the interferometer arms. As we will see, for ground based interferometers this is of the order 10^2 kms. Therefore, in different detectors, very different values of $S_\xi(\omega)$ can correspond to the same minimum value of $\tilde{h}(\omega)$ that can be measured.

the fact that it produces a stochastic force, responsible both for the dissipation term $-\gamma_0\dot{\xi}_0$, and for fluctuations around it. To take fluctuations into account the above equation must be replaced by

$$m_0(\ddot{\xi}_0 + \omega_0^2\xi_0) = F_{\rm stoc} \tag{8.109}$$

with

$$\langle F_{\rm stoc}\rangle = -m_0\gamma_0\dot{\xi}_0\,. \tag{8.110}$$

We write $F_{\rm stoc} = -m_0\gamma_0\dot{\xi}_0 + F(t)$, where $F(t)$ is a stochastic force that describes the thermal fluctuations, known as the Nyquist force. By definition $\langle F(t)\rangle = 0$. Thermal noise fluctuations can be described by a stochastic Gaussian process, since they are the sum of many independent contributions, so the stochastic properties of $F(t)$ are uniquely defined by its average value that, as we have seen, is zero, and by its auto-correlation function $\langle F(t)F(t')\rangle$. At the microscopic level, $F(t)$ is due to atomic collisions, at a rate which can be, say, $O(10^{19})$ collisions per second. Therefore, on a macroscopic time-scale, the force at time t and at time t' are completely uncorrelated if $t \neq t'$, and we can write

$$\langle F(t)F(t')\rangle = A_0\delta(t-t')\,. \tag{8.111}$$

We will see in a moment how to fix the constant A_0. The dynamics of $\xi_0(t)$ is now governed by

$$\ddot{\xi}_0 + \gamma_0\dot{\xi}_0 + \omega_0^2\xi_0 = \frac{F(t)}{m_0}\,, \tag{8.112}$$

which has the solution

$$\xi_0(t) = \xi_0^{\rm hom}(t) + \frac{1}{m_0}\int_{-\infty}^{\infty} dt'\, G(t-t')F(t')\,, \tag{8.113}$$

where $\xi_0^{\rm hom}(t)$ is the general solution of the homogeneous equation and $G(t)$ is a Green's function, i.e. a solution of eq. (8.112) with $F(t)/m_0$ replaced by $\delta(t)$. The Green's function can be easily found performing the Fourier transform and repeating basically the same steps that lead to the integration of eq. (8.22),[26] and we get

$$G(t) = \frac{1}{\omega_0}\theta(t)e^{-\gamma_0 t/2}\sin\omega_0 t\,, \tag{8.114}$$

where $\theta(t)$ is the step function, $\theta(t) = 0$ for $t < 0$ and $\theta(t) = 1$ for $t > 0$. Therefore

$$\xi_0(t) = \xi_0^{\rm hom}(t) + \frac{1}{m_0\omega_0}\int_{-\infty}^{t} dt' e^{-\gamma_0(t-t')/2}\sin[\omega_0(t-t')]F(t')\,. \tag{8.115}$$

We assume for simplicity that $F(t)$ is switched on at $t = 0$, and that $\xi_0(0) = 0$ and $\dot{\xi}(0) = 0$. With these boundary conditions we get, for $t > 0$,

$$\xi_0(t) = \frac{1}{m_0\omega_0}\int_0^t dt'\, e^{-\gamma_0(t-t')/2}\sin[\omega_0(t-t')]F(t')\,. \tag{8.116}$$

[26] The Green's function is selected uniquely imposing the causality condition, i.e. requiring that the particular solution of the inhomogeneous equation, at time t, depends only on $F(t')$ at $t \leqslant t$.

Using eq. (8.111) and introducing $u = t - t'$ we then obtain

$$\begin{aligned}\langle\xi_0^2(t)\rangle &= \frac{A_0}{m_0^2\omega_0^2}\int_0^t du\, e^{-\gamma_0 u}\sin^2\omega_0 u \\ &\simeq \frac{A_0}{2m_0^2\omega_0^2\gamma_0}(1-e^{-\gamma_0 t})\,,\end{aligned} \tag{8.117}$$

where in the last line we neglected terms which are small for $\gamma_0 \ll \omega_0$. The time evolution of the average kinetic plus potential energy of the mode ξ_0 due to thermal noise is therefore given by

$$\begin{aligned}\langle E(t)\rangle &= \frac{1}{2}m_0\omega_0^2\langle\xi_0^2\rangle + \frac{1}{2}m_0\langle\dot{\xi}_0^2\rangle \\ &= m_0\omega_0^2\langle\xi_0^2\rangle \\ &\simeq \frac{A_0}{2m_0\gamma_0}(1-e^{-\gamma_0 t})\,.\end{aligned} \tag{8.118}$$

In the limit $t \to \infty$, the system thermalizes and the equipartition of energy states that $\langle E_{\rm kin}(t)\rangle \to (1/2)kT$ and $\langle E_{\rm pot}(t)\rangle \to (1/2)kT$, so $\langle E(t)\rangle \to kT$. Comparison with eq. (8.118) fixes the value of A_0,

$$A_0 = 2kT\, m_0\gamma_0\,, \tag{8.119}$$

and therefore

$$\langle E(t)\rangle = kT(1-e^{-t/\tau_0})\,, \tag{8.120}$$

where $\tau_0 = 1/\gamma_0$. This shows that, while asymptotically $\langle E(t)\rangle \to kT$, equilibrium is reached only on a time-scale $t \gg \tau_0$. On a time-scale $\Delta t \ll \tau_0$, expanding the exponential in eq. (8.120) we rather get

$$\langle E(t=\Delta t)\rangle \simeq kT\,\frac{\Delta t}{\tau_0}\,, \tag{8.121}$$

confirming the physical intuition that led to eq. (8.107). It is instructive to realize that the result (8.119) is a particular case of a very general theorem. According to the definition (7.15), which expresses in general the relation between the spectral density and the auto-correlation function of any quantity, the (single-sided) spectral density of the force $F(t)$, that we denote by $S_F(\omega)$, is related to the auto-correlation function of $F(t)$, $R_F(t'-t) \equiv \langle F(t')F(t)\rangle$, by

$$\langle F(t')F(t)\rangle = \frac{1}{2}\int_{-\infty}^{\infty}\frac{d\omega}{2\pi}\,S_F(\omega)e^{-i\omega(t'-t)}\,. \tag{8.122}$$

Comparison with eq. (8.111) shows that $S_F(\omega) = 2A_0$, so the spectral density is flat. Equation (8.119) can therefore be seen as a relation between the fluctuations due to the force F (represented by S_F) and the dissipation (represented by γ_0),

$$S_F = 4kT\, m_0\gamma_0\,. \tag{8.123}$$

This result is a particular case of the *fluctuation–dissipation theorem*, which can be formulated as follows. Let $x(t)$ by a variable describing

a linear system (either mechanical or electrical) subject to an external force $F(t)$, and let $v(t) = \dot{x}(t)$ be the velocity. In Fourier space, we can always cast the equation of motion of a linear system in the general form

$$\tilde{F}(\omega) = Z(\omega)\tilde{v}(\omega)\,. \tag{8.124}$$

This defines the impedance $Z(\omega)$. Its inverse, $Y(\omega) = Z^{-1}(\omega)$, is called the admittance. The fluctuation–dissipation theorem states that the (single-sided) power spectrum of the force responsible for thermal fluctuations, $S_F(\omega)$, is related to the real part of Z by

$$\boxed{S_F(\omega) = 4kT\ \mathrm{Re}\, Z(\omega)\,.} \tag{8.125}$$

For the damped oscillator, eq. (8.112) gives

$$Z = -\frac{im_0}{\omega}(\omega^2 - \omega_0^2 + i\gamma_0\omega)\,, \tag{8.126}$$

so Re $Z = m_0\gamma_0$ and we recover eq. (8.123). The real part of Z in general is responsible for dissipation in the system, so eq. (8.125) relates fluctuations to dissipation.

We can now compute the spectral density of the noise due to thermal fluctuations, considering for the moment only the bar's mode ξ_0. Below we will generalize to the bar–transducer system. Writing the velocity as $\tilde{v}(\omega) = -i\omega\tilde{\xi}_0(\omega)$, eq. (8.124) can be written as

$$\tilde{\xi}_0(\omega) = \frac{1}{-i\omega Z(\omega)}\,\tilde{F}(\omega)\,, \tag{8.127}$$

and therefore

$$\begin{aligned} S_\xi^{\mathrm{thermal}}(\omega) &= \frac{1}{\omega^2|Z(\omega)|^2}S_F(\omega) \\ &= \frac{4kT\,m\gamma_0}{\omega^2|Z(\omega)|^2}\,. \end{aligned} \tag{8.128}$$

From the explicit forms (8.126) and (8.23) we see that $Z(\omega)$ is related to the transfer function of the mode ξ_0, $T_0(\omega)$, by

$$T_0(\omega) = \frac{2L}{\pi^2}\,\frac{m_0\omega}{iZ(\omega)}\,. \tag{8.129}$$

Therefore we can rewrite eq. (8.128) as

$$S_\xi^{\mathrm{thermal}}(\omega) = \frac{4kT\,\gamma_0}{m_0\omega^4}\left(\frac{\pi^2}{2L}\right)^2 |T_0(\omega)|^2\,. \tag{8.130}$$

The contribution to the noise spectral density due to the thermal noise is obtained using eq. (8.106). We see that $|T(\omega)|^2$ cancels, and we end up with

$$\boxed{S_n^{\mathrm{thermal}}(f) = \frac{\pi}{Q_0}\,\frac{kT}{Mv_s^2}\,\frac{f_0^3}{f^4}\,,} \tag{8.131}$$

where we eliminated L using $\omega_0 = \pi v_s/L$, with v_s the speed of sound in the bar, we used $m_0 = M/2$, with M the total mass of the bar, $\gamma_0 = \omega_0/Q_0$, and we expressed everything in terms of $f = \omega/(2\pi)$. We can make the following comments.

- We have found that $S_\xi^{\mathrm{thermal}}(\omega)$ is proportional to $|T_0(\omega)|^2$. Since however the contribution of thermal noise to $S_n(\omega)$ is obtained dividing $S_\xi^{\mathrm{thermal}}(\omega)$ by $|T_0(\omega)|^2$, see eq. (8.106), the transfer function $T_0(\omega)$ cancels, and $S_n(f)$ shows no special feature around the resonance frequency f_0; rather, it has a smooth frequency dependence, $S_n(f) \sim f^{-4}$. This means that, if thermal noise were the only source of noise, resonant bars would be wide-band detectors, that is, their sensitivity would not be limited to a region close to f_0. As we will see below, bars become narrow-band detectors only when we include the noise introduced by the read-out scheme.
- We understand the importance of a large quality factor, since we found $S_n^{\mathrm{thermal}}(f) \sim 1/Q_0$. This is in agreement with eq. (8.107), since $\tau_0 = Q_0/\omega_0$, so $(\Delta E_{\mathrm{min}})_{\mathrm{thermal}} \sim 1/Q_0$. Furthermore, we learn from eq. (8.131) that thermal noise can be fought lowering T (obviously), but also taking M and v_s as large as possible. The dependence $1/M$ expresses the physically obvious fact that thermal noise is not effective in generating a coherent motion of a massive object. We also see that $S_n^{\mathrm{thermal}}(f)$ decreases at high frequencies, but this result will be modified when we include the transducer.

The computation of the noise spectral density performed above takes into account only the bar mode ξ_0. We now consider the bar–transducer system, and we compute the effect of thermal noise on the transducer displacement. At first sight, eq. (8.131) can be alarming, because it suggests that, if the thermal noise of the bar is proportional to $1/M$, the thermal noise of the transducer should be proportional to $1/m_{\mathrm{t}}$, and therefore it will be very large, since the transducer is very light. This would ruin completely the usefulness of the resonant transducer scheme. However, eq. (8.131) has been derived for a single oscillator, while here we have two coupled oscillators. We now show that it is indeed correct that, in the bar–transducer system, the thermal noise in the transducer is $S_n(f) \sim 1/m_{\mathrm{t}}$, except in a narrow frequency range around the resonant frequency. This will provide a first (but, as it turns out, not the most important) reason that limits the bandwidth of resonant bar detectors.

To this end, we go back to eq. (8.93), which gives the transducer displacement $\tilde{\xi}_{\mathrm{t}}(\omega)$, when we apply a force F_0 on the bar and a force F_{t} on the transducer. In terms of the transfer function given in eq. (8.95) we can write

$$\tilde{\xi}_{\mathrm{t}}(\omega) = -\frac{\pi^2}{2L}\,\frac{T_{\mathrm{t}}(\omega)}{\omega^2}\left[\frac{\tilde{F}_0(\omega)}{m_0} - \frac{\tilde{F}_{\mathrm{t}}(\omega)}{m_{\mathrm{t}}}\,\frac{\omega^2 - \omega_0^2 + i\omega\gamma_0}{\omega_0^2}\right]. \tag{8.132}$$

To compute the effect of thermal noise, we take as F_0 and F_{t} the Nyquist forces acting on the bar's fundamental mode and on the transducer,

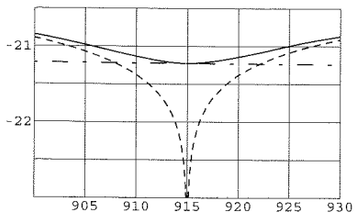

Fig. 8.8 $\log_{10}[S_n^{\rm thermal}(f)]^{1/2}$, as a function of the frequency f (in Hz). Dashed line: transducer contribution. Dot-dashed: bar contribution. Solid line: total thermal noise. We use as numerical values $Q_0 = Q_{\rm t} = 2\times10^6$, $T = 1$ K, $M = 2300$ kg, $L = 3$ m, $v_s = 5400$ m/s, $f_0 = 915$ Hz, $\mu = 2.4\times10^{-4}$.

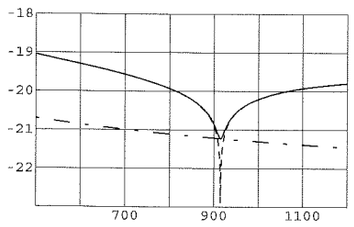

Fig. 8.9 The same as Fig. 8.8, on a larger frequency range.

respectively. From the fluctuation–dissipation theorem, in the form of eq. (8.123), we have

$$S_{F_0} = 4kT\, m_0\gamma_0\,, \qquad S_{F_{\rm t}} = 4kT\, m_{\rm t}\gamma_{\rm t}\,. \tag{8.133}$$

Assuming that the Nyquist forces acting on the bar and on the transducer are uncorrelated we find, for the spectral density of the transducer displacement,

$$S_{\xi_{\rm t}}(\omega) = \frac{\pi^4}{4L^2}\,\frac{|T_{\rm t}(\omega)|^2}{\omega^4}\,4kT\left[\frac{\gamma_0}{m_0} + \frac{\gamma_{\rm t}}{m_{\rm t}}\,\frac{(\omega^2-\omega_0^2)^2+\omega^2\gamma_0^2}{\omega_0^4}\right]. \tag{8.134}$$

As discussed above, the noise spectral density is obtained dividing by $|T_{\rm t}(\omega)|^2$, so we get (using $L = \pi v_s/\omega_0$, $m_0 = M/2$, $\gamma_0 = \omega_0/Q_0$, $\gamma_{\rm t} = \omega_0/Q_{\rm t}$ and expressing the result in terms of $f = \omega/2\pi$)

$$S_n^{\rm thermal}(f) = \pi\,\frac{kT}{Mv_s^2}\,\frac{f_0^3}{f^4}\left[\frac{1}{Q_0} + \frac{1}{\mu Q_{\rm t}}\,\frac{(f^2-f_0^2)^2+(ff_0/Q_0)^2}{f_0^4}\right]. \tag{8.135}$$

The term $1/Q_0$ in the bracket is the thermal noise of the bar, see eq. (8.131). The second term is the transducer thermal noise, and we see that it is indeed proportional to $1/m_{\rm t}$, so it is enhanced by a factor $1/\mu$ compared to the bar's noise. What saves the situation is the fact that $1/m_{\rm t}$ is multiplied by a function of f which becomes very small at $f = f_0$,

$$S_n^{\rm thermal}(f_0) = \frac{\pi}{Q_0}\,\frac{kT}{Mv_s^2}\,\frac{f_0^3}{f^4}\left[1+\frac{1}{\mu Q_{\rm t}Q_0}\right]. \tag{8.136}$$

Numerically, for $Q_0 \sim Q_{\rm t} \sim 10^6$ and $\mu = 10^{-4}$, we have $1/(\mu Q_{\rm t}Q) \sim 10^{-8}$, so at $f = f_0$ the transducer thermal noise is completely negligible, and it remains smaller or of the same order of magnitude of the bar's thermal noise as long as $(f^2-f_0^2)^2/f_0^4 \leqslant \mu(Q_{\rm t}/Q_0)$, or, since $(Q_{\rm t}/Q_0) = O(1)$, as long as $|f-f_0| \lesssim f_0\sqrt{\mu}$.

We see that the term $(ff_0/Q)^2$ in eq. (8.135) gives a totally negligible contribution to $S_n^{\rm thermal}(f)$ even when $f^2-f_0^2 = 0$, so we can neglect it everywhere, and we can write more simply

$$\boxed{S_n^{\rm thermal}(f) = \pi\,\frac{kT}{Mv_s^2}\,\frac{f_0^3}{f^4}\left[\frac{1}{Q_0} + \frac{1}{\mu Q_{\rm t}}\,\frac{(f^2-f_0^2)^2}{f_0^4}\right].} \tag{8.137}$$

In Fig. 8.8 we plot the function $[S_n^{\rm thermal}(f)]^{1/2}$, and the two separate contributions from the bar and the transducer. With the parameters given in the figure caption, at $f = f_0$ we get $\left[S_n^{\rm thermal}(f_0)\right]^{1/2} \simeq 6\times10^{-22}\,{\rm Hz}^{-1/2}$. Observe that the thermal noise is minimum at f_0, rather than at the normal mode frequencies $f_\pm$. Figure 8.9 shows the same quantities on a larger frequency window. Observe also that, at low f, $S_n^{\rm thermal}(f)$ diverges as $1/f^4$, while at large f it goes to a constant.

8.3.2 Read-out noise and effective temperature

We now consider the other crucial source of noise in resonant detectors, that is, the noise introduced by the read-out scheme. We have seen that the output of a capacitive transducer is a potential, V, which is modulated by the displacement of the light mass, as in eq. (8.97), and further amplified electronically. Any amplifier has however an associated wideband noise, described by a spectral density of the output potential, S_V approximately constant in frequency, and with dimensions volts^2/Hz. Since $V = \alpha\xi_{\rm t}$, any fluctuation in the potential due to electronic noise results in an error in the measurement of $\xi_{\rm t}$, which can be described by a spectral density of the displacement

$$S_{\xi_{\rm t}}^{\rm ampl} = \frac{1}{\alpha^2}\,S_V\,. \tag{8.138}$$

With good approximation α and S_V are independent of the frequency in the bandwidth of interest, so $S_{\xi_{\rm t}}^{\rm ampl}$ is approximately a white noise. Observe also that $S_{\xi_{\rm t}}^{\rm ampl}$ can be made smaller increasing α, that is, transferring more efficiently the energy from the mechanical oscillators to the amplifier.

As we did for thermal noise, we can characterize the amplifier noise either in terms of the energy that must be deposited by a GW burst in order to overcome it, or in terms of the noise spectral density. We consider first the energetic point of view. If, as in eq. (8.107), we use a sampling time Δt, the bandwidth is $\Delta f \simeq 1/\Delta t$. Then the fluctuations in $\xi_{\rm t}^2$ due to amplifier noise in such a sampling time are given by

$$\langle\xi_{\rm t}^2(t)\rangle = \int_{f_0-\Delta f/2}^{f_0+\Delta f/2} df\, S_{\xi_{\rm t}}^{\rm ampl} = S_{\xi_{\rm t}}^{\rm ampl}\Delta f\,. \tag{8.139}$$

The corresponding minimum value of the detectable energy is therefore given by

$$\boxed{(\Delta E_{\rm min})_{\rm ampl} = m_{\rm t}\omega_0^2\langle\xi_{\rm t}^2(t)\rangle \simeq m_{\rm t}\omega_0^2 S_{\xi_{\rm t}}^{\rm ampl}\,\frac{1}{\Delta t}\,.} \tag{8.140}$$

We see that $(\Delta E_{\rm min})_{\rm ampl}$ is proportional to $1/\Delta t$. This is due to the fact that, if the sampling time is small, the bandwidth is large and we are flooded with amplifier noise. On the contrary, we saw in eq. (8.107) that $(\Delta E_{\rm min})_{\rm thermal}$ is proportional to Δt. Therefore, putting together the amplifier and thermal noise, we discover that there is an optimum value of the sampling time Δt and therefore of the bandwidth. We come back to this below

The other useful (and more detailed) characterization of amplifier noise is in terms of its noise spectral density, $S_n^{\rm ampl}(f)$. According to the general definition (8.106), to get $S_n^{\rm ampl}$ we must divide the spectral density of the transducer displacement, $S_{\xi_{\rm t}}^{\rm ampl}$ by the squared modulus of the transducer transfer function $T_{\rm t}(\omega)$, given in eq. (8.95). Recalling

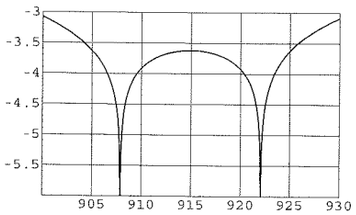

Fig. 8.10 $\log_{10}[S_n^{\rm ampl}(f)/\mathcal{A}]^{1/2}$, as a function of the frequency, for $\mu = 2.4 \times 10^{-4}$ and $f_0 = 915$ Hz.

that $\bar\gamma = \omega_0/Q_m$, see eq. (8.96), we get

$$\boxed{S_n^{\rm ampl}(f) = \mathcal{A}\,\frac{\left[(f^2-f_+^2)^2+(ff_0/Q_m)^2\right]\left[(f^2-f_-^2)^2+(ff_0/Q_m)^2\right]}{f^4 f_0^4}}, \tag{8.141}$$

where

$$\mathcal{A} = \frac{\pi^4}{4L^2}\,S_{\xi_{\rm t}}^{\rm ampl}\,. \tag{8.142}$$

In Fig. 8.10 we show the dimensionless quantity $[S_n^{\rm ampl}(f)/\mathcal{A}]^{1/2}$, for the same values of f_0, μ, Q_0 and $Q_{\rm t}$ used above for thermal noise. The amplifier thermal noise is minimum at the two resonance frequencies $f_\pm$.

Thermal and amplifier noise are the two dominant contributions to the strain sensitivity in present detectors, so we can now put these two effects together and obtain a first understanding of the detector's sensitivities. We start from the energy considerations, that are less accurate (since the detailed frequency dependence is integrated over) but more intuitive. Combining eqs. (8.107) and (8.140) we see that the minimum detectable energy is

$$\Delta E_{\rm min} \sim kT\,\frac{\Delta t}{\tau} + m_{\rm t}\omega_0^2 S_{\xi_{\rm t}}^{\rm ampl}\,\frac{1}{\Delta t}\,, \tag{8.143}$$

where Δt is the sampling time. We take τ to be the relaxation time of the full three modes system (mechanical plus electric), and we write $\tau = Q/\omega_0$, where Q is the overall quality factor of the system. Since the first term is proportional to Δt and the second to $1/\Delta t$, we can minimize $\Delta E_{\rm min}$ choosing an optimal value of Δt. This gives

$$\Delta f \simeq \frac{1}{(\Delta t)_{\rm opt}} \sim \pi\frac{f_0}{Q}\,\Gamma^{-1/2}\,. \tag{8.144}$$

where

$$\Gamma = \frac{m_{\rm t}\omega_0^3 S_{\xi_{\rm t}}^{\rm ampl}}{4QkT}\,, \tag{8.145}$$

In typical experimental situations, we can have $Q = O(10^6)$ and $\Gamma = O(10^{-8}$–$10^{-9})$. Therefore, at a frequency $f_0 \simeq 1$ kHz, we can have $\Delta f = O(10$–$100)$ Hz. An important point that we understand from this result (and which was fully realized only in the 1980s) is that the useful bandwidth of a resonant bar has nothing to do with the width of the peak of the resonance in the transfer function. In fact, the latter is $(\Delta f)_{\rm res} = f_0/Q$ and, for typical values $Q \sim 10^6$ and $f_0 \sim 1$ kHz, it is extremely small, of order of 1 mHz. Instead the useful bandwidth, given in eq. (8.144), is many order of magnitude larger: it depends on Q only as $1/Q^{1/2}$ rather than as $1/Q$ (since $\Gamma \sim 1/Q$), and we see from eq. (8.145) that it can be made larger lowering the amplifier noise, so it really depends on the details of the read-out system.[27]

When $\Delta t = (\Delta t)_{\rm opt}$, the two terms on the right-hand side of eq. (8.143) become equal, and

$$\Delta E_{\rm min} \sim 2kT\,\frac{(\Delta t)_{\rm opt}}{\tau}\,. \tag{8.146}$$

[27] Observe also that $S_{\xi_{\rm t}}^{\rm ampl}$ is proportional to $1/\alpha^2$, see eq. (8.138), and therefore to $1/\beta^2$, see eq. (8.101). Therefore eq. (8.145) show that Γ is proportional to $1/\beta^2$ and, from eq. (8.144), Δf is proportional to β. Therefore the bandwidth can be enlarged increasing β, i.e. the coupling of the mechanical to the electric modes, compare with Note 20 on page 434.

Writing $(\Delta t)_{\rm opt} \sim 1/\Delta f$ and $1/\tau_0 = \gamma_0 = \omega_0/Q$, we get

$$\Delta E_{\rm min} = kT_{\rm eff}\,, \tag{8.147}$$

with an *effective temperature* $T_{\rm eff}$ given by

$$\boxed{T_{\rm eff} \sim \frac{4\pi}{Q}\,\frac{f_0}{\Delta f}\,T \simeq 4\Gamma^{1/2}T\,.} \tag{8.148}$$

For a bar cooled at a thermodynamic temperature $T \simeq 2$ K, with $Q \simeq 1\times 10^6$, $\Delta f \simeq 10$ Hz, $f_0 \simeq 900$ Hz, eq. (8.148) gives $T_{\rm eff} \simeq 2$ mK. This result is quite interesting; it means that, even in a bar at the thermodynamical temperature of 2 K, we can detect bursts that deposited in it an energy E_s of just a few mK. The fact that, sampling the output at a fast rate, we can dig deeply into thermal noise, is of course just an example of the general concept of matched filtering that we discussed in Section 7.3.

To have a more detailed picture, we consider now the noise spectral density. The total noise spectral density is

$$S_n(f) = S_n^{\rm thermal}(f) + S_n^{\rm ampl}(f)\,, \tag{8.149}$$

with $S_n^{\rm thermal}(f)$ is the spectral density of thermal noise (bar plus transducer) given in eq. (8.137) and $S_n^{\rm ampl}(f)$ is the spectral density of the amplifier noise given in eq. (8.141). The total strain sensitivity is $S_n^{1/2}(f)$. Explicitly, recalling that $\mu = m_{\rm t}/m = 2m_{\rm t}/M$, we have

$$S_n(f) = \frac{\pi kT}{Mv_s^2 f_0}\left\{\frac{f_0^4}{f^4}\left[\frac{1}{Q_0}+\frac{1}{\mu Q_{\rm t}}\,\frac{(f^2-f_0^2)^2}{f_0^4}\right]\right. \tag{8.150}$$
$$\left. + \frac{Q\Gamma}{\mu}\,\frac{\left[(f^2-f_+^2)^2+(ff_0/Q_m)^2\right]\left[(f^2-f_-^2)^2+(ff_0/Q_m)^2\right]}{f^4 f_0^4}\right\}.$$

We recall that Q_0, Q_t are the quality factors of the fundamental mode of the bar ξ_0 and of the transducer $\xi_{\rm t}$, respectively; Q_m is the total mechanical quality factor, see eq. (8.96) and Q, which enters in the definition (8.145) of Γ, is the total quality factor of the system.

We see that, for given values of the quality factors and of μ, the factor Γ determines the relative importance of thermal and read-out noise, and therefore controls the bandwidth Δf.

In Figs. 8.11–8.13 we plot the logarithm of the total strain sensitivity $[S_n(f)]^{1/2}$ (solid line) and the separate contribution from thermal noise of the bar and of the transducer $[S_n^{\rm thermal}(f)]^{1/2}$ (dot-dashed line), and from the amplifier noise, $[S_n^{\rm ampl}(f)]^{1/2}$ (dashed line). We use for definiteness the values $\mu = 2.4\times 10^{-4}$, $Q_0 = Q_{\rm t} = Q = 2\times 10^6$, $T = 1$ K, $M = 2300$ kg, $v_s = 5400$ m/s, $f_0 = 915$ Hz, and we vary Γ, so we change the relative importance of amplifier and thermal noise.

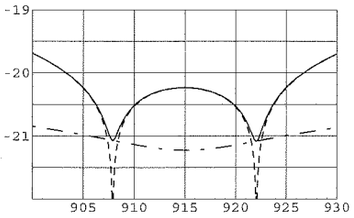

Fig. 8.11 $\log_{10}[S_n^{1/2}]$ as a function of the frequency, in Hz, taking $\Gamma = 10^{-7}$. The other parameters are given in the text. Dashed line: amplifier noise. Dot-dashed line: thermal noise (bar plus transducer). Solid line: total. Here the amplifier noise dominates, except very close to the resonances.

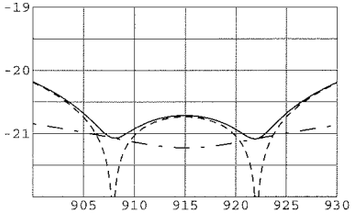

Fig. 8.12 The same as Fig. 8.11, but with $\Gamma = 10^{-8}$. Thermal and amplifier noise are comparable.

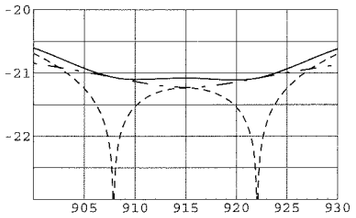

Fig. 8.13 The same as Fig. 8.11, but with $\Gamma = 10^{-9}$. Now thermal noise dominates (which means that one has chosen a transducer too light).

8.3.3 Back-action noise and the quantum limit

In this section we discuss another source of intrinsic noise, the *back-action* noise, that in present resonant detectors is small, but which can become important for the design of advanced detectors, and also has an intrinsic conceptual interest, because of its relation with fundamental limitations imposed by quantum mechanics.

When we studied the double oscillator, in Section 8.2.1, we introduced external forces acting on the oscillator ξ_0 (which represents the fundamental mode of the bar) and on the oscillator ξ_t, which represents the light mass, and we denoted these forces by F_0 and F_t respectively. We then wrote the equations of motion in the form (8.72)–(8.73). Furthermore, we had an elastic force acting *between* the bar and the light mass. Defining the spring constant $k = m_t\omega_t^2$, eqs. (8.72) and (8.73) can be rewritten as

$$m(\ddot{\xi}_0 + \omega_0^2\xi_0) = +k(\xi_t - \xi_0) + F_0\,, \tag{8.151}$$
$$m_t\ddot{\xi}_t = -k(\xi_t - \xi_0) + F_t\,. \tag{8.152}$$

Of course, since the force $k(\xi_t - \xi_0)$ acts between the bar and the light mass, it enters with opposite signs in the equations for $\ddot{\xi}_0$ and for $\ddot{\xi}_t$.

As we saw in Section 8.2.2, this coupling between ξ_0 and ξ_t is a schematization of an extended device which consists of a capacitor, which in turn is part of an LC circuit, and is connected to an amplifier. This read-out has been designed so that the mechanical oscillations of the transducer are transformed into an electric signal. Unfortunately this process is reversible, and fluctuations in the electric circuit generate a force that actually shakes the transducer and the bar. Any noise in the electronic apparatus will then appear as a stochastic force F_{0t} acting *between* the bar and the light mass. This force is called the back-action exerted on the bar and on the light mass by the amplifier. More generally, it describes the effect of any fluctuation taking place between the bar and the transducer, e.g. fluctuations of the electric field in the capacitor. Then eqs. (8.151) and (8.151) must rather be written as

$$m(\ddot{\xi}_0 + \omega_0^2\xi_0) = +k(\xi_t - \xi_0) + F_{0t} + F_0\,,$$
$$m_t\ddot{\xi}_t = -k(\xi_t - \xi_0) - F_{0t} + F_t\,, \tag{8.153}$$

or, including also the dissipation terms as in eqs. (8.88) and (8.89),

$$m(\ddot{\xi}_0 + \omega_0^2\xi_0) = +k(\xi_t - \xi_0) + [F_{0t} + m_t\gamma_t(\dot{\xi}_t - \dot{\xi}_0)] + [F_0 - m\gamma_0\dot{\xi}_0]\,,$$
$$m_t\ddot{\xi}_t = -k(\xi_t - \xi_0) - [F_{0t} + m_t\gamma_t(\dot{\xi}_t - \dot{\xi}_0)] + F_t\,. \tag{8.154}$$

Having extracted explicitly these dissipation terms, now F_0 and F_{0t} are stochastic forces with zero mean, $\langle F_{0t}\rangle = \langle F_0\rangle = 0$, characterized by their spectral densities S_{F_0} and $S_{F_{0t}}$. (Since we are studying the noise acting on the bar, we can assume that there is no GW contribution to F_0; otherwise, we can just extract the GW force and write it explicitly.) Then the spectral densities of eq. (8.133) must be replaced by

$$S_{F_0} \to S_{F_0} + S_{F_{0t}}\,, \qquad S_{F_t} \to S_{F_t} + S_{F_{0t}}\,. \tag{8.155}$$

To evaluate $S_{F_{0t}}$ we consider for instance the case of a voltage amplifier.[28] In a voltage amplifier the noise can be described by a voltage noise plus independent fluctuations in the current. We denote the single-sided spectral densities of the voltage and current noise by v_n^2 (measured in volts^2/Hz) and i_n^2 (in amp^2/Hz), respectively. The spectral density of the output voltage V is given by $S_V = v_n^2 + |Z|^2 i_n^2$, where Z is the impedance, and we neglected correlated noise between voltage and current. It is customary to define the noise temperature T_n of the amplifier by $2kT_n = v_n i_n$ (where the factor of 2 is due to the fact that we use single-side spectral densities), and the amplifier noise resistance $R_n = v_n/i_n$. Introducing further the dimensionless quantity $\lambda = R_n/|Z|$, known as the impedance match ratio, and using eq. (8.101), one gets

$$S_{\xi_t}^{\rm ampl} = \frac{1}{\alpha^2}\,(v_n^2 + |Z|^2 i_n^2)$$
$$= \frac{2kT_n}{m_t\omega_0^3\beta}\left(\lambda + \frac{1}{\lambda}\right)\,. \tag{8.156}$$

The back-action force due to current fluctuations can be computed in this case observing that the power dissipated in the electric circuit is $P = VI$. The contribution to V due to the displacement of the transducer is obtained from eq. (8.98), $V = Z_{21}\dot{\xi}_t$, so the corresponding power is $P = Z_{21}I\dot{\xi}_t$. This is the power generated by a force of modulus $Z_{21}I$ acting on a mechanical object with velocity $\dot{\xi}_t$. Therefore a current I in the circuit exerts on the transducer a force of modulus $F_{0t} = Z_{21}I$, and the spectral density of this back-action force is $S_{F_{0t}} = |Z_{21}|^2\, i_n^2$, where i_n is the spectral density of the current. As we saw below eq. (8.98), $|Z_{21}| = \alpha/\omega_0$, so $S_{F_{0t}} = \alpha^2 i_n^2/\omega_0^2$. In terms of T_n and λ, we have $i_n^2 = 2kT_n/\lambda|Z|$, and therefore

$$S_{F_t} + S_{F_{0t}} = 4kT\, m_t\gamma_t + 2kT_n\,\frac{\alpha^2}{\omega_0^2\lambda|Z|}\,. \tag{8.157}$$

Expressing the result in terms of β, given in eq. (8.102), we find

$$S_{F_t} + S_{F_{0t}} = 4\, m_t\gamma_t\left(kT + kT_n\frac{\beta Q_t}{2\lambda}\right)\,. \tag{8.158}$$

Therefore, at least in a first approximation,[29] the back action is formally equivalent to a shift of the transducer temperature

$$\boxed{T \to T + \frac{\beta Q_t}{2\lambda}T_n\,.} \tag{8.159}$$

For the amplifier noise we use eq. (8.156). Typically $\lambda \gg 1$ so, $S_{\xi_t}^{\rm ampl} \simeq 2kT_n\lambda/m_t\omega_0^3\beta$. Then, including the back-action, the minimum detectable energy (8.143) becomes

$$\Delta E_{\rm min} \sim \left(kT + \frac{\beta Q}{2\lambda}kT_n\right)\,\frac{\Delta t}{\tau} + \frac{2kT_n\lambda}{\beta\omega_0\Delta t}\,. \tag{8.160}$$

[28] This example is somewhat old-fashioned, since modern resonant detectors use SQUIDS rather than voltage amplifiers, but is the simplest setting for illustrating the general ideas.

[29] A more detailed computation based on the full set of equations governing the coupled mechanical and electric modes show that the strain sensitivity of the back-reaction has a different form, as a function of the frequency, from that due to thermal noise.

This expression raises an interesting issue of principle because it shows that, even if one were able to cool the bar to a negligibly small value of the thermodynamic temperature T, still there would be a minimum value of the detectable energy, since even at $T = 0$ we have both a term proportional to Δt and a term proportional to $1/\Delta t$. Setting $T = 0$ in eq. (8.160) and writing $\tau = Q/\omega_0$, we have

$$\Delta E_{\min} \sim kT_n \left(\frac{\beta\omega_0}{2\lambda}\,\Delta t + \frac{2\lambda}{\beta\omega_0}\,\frac{1}{\Delta t} \right) . \tag{8.161}$$

This is minimized choosing $(\Delta t)_{\rm opt} = 2\lambda/(\beta\omega_0)$, and the corresponding minimum detectable value of the energy is

$$\Delta E_{\min} \sim 2kT_n\,. \tag{8.162}$$

Therefore, even if we cool the detector to T close to zero, an ultimate limitation is provided by the amplifier noise temperature. For a SQUID, $T_n \sim 10^{-3}$ mK, while the lowest effective temperatures that have been reached by bars at present are of the order of 0.3 mK, so this limit at present is not very important from a practical point of view.

Nevertheless, this observation brings us to a second interesting question, namely, what is the minimum value that can be obtained in principle for the amplifier noise temperature T_n? As we will discuss in the next subsection (and as was shown by Heffner, already in 1962) any linear amplifier (e.g. an object that preserves a linear relation between the input and output values of the amplitude and the phase of the signal) working at a frequency ω_0, as a consequence of the uncertainty principle, has a minimum noise temperature given by

$$kT_n \sim \hbar\omega_0\,. \tag{8.163}$$

We therefore discover that the ultimate limitation for a resonant bar operating with a linear amplifier is given by the uncertainty principle,

$$\boxed{\Delta E_{\min} \gtrsim \hbar\omega_0\,.} \tag{8.164}$$

This is known as the *standard quantum limit*. It states that the best we can do (with a linear amplifier) is to detect an acoustic oscillation of the fundamental mode of the bar which, at the quantum level, corresponds to a single phonon.

A measure of how far we are presently from the quantum limit is provided by

$$N_{\rm phonon} = \frac{kT_{\rm eff}}{\hbar\omega_0}\,. \tag{8.165}$$

For $T_{\rm eff} \simeq 2$ mK and $f_0 = 900$ Hz, $N_{\rm phonon} \simeq 5 \times 10^4$. Both the group that runs the EXPLORER and NAUTILUS detectors and the AURIGA group have attained $N_{\rm phonon} \simeq 10^2$ so, for the moment, the quantum limit is not the main limitation in resonant bars, although we are getting closer to it. The detection of a single-phonon excitation in a two-ton bar would be a remarkable technical achievement, and would correspond to an energy detection sensitivity at the level $\hbar\omega_0 \simeq 6 \times 10^{-31}$ J.

Further reflection shows that the quantum limit, in itself, cannot be an absolute limit. Quantum mechanics does not forbid arbitrarily precise measurements of energy, but only arbitrarily precise simultaneous measurements of conjugate variables. The origin of the problem is that a linear amplifier allows us to reconstruct both the amplitude and the phase of the motion of the oscillator $\xi_{\rm t}$. However, for a harmonic oscillator, to know its amplitude and its phase is equivalent to knowing simultaneously the position and the momentum, and it is here that the Heisenberg principle comes into play. The quantum limit can therefore be evaded if we give up the information on the phase. We discuss the issue in more detail in the next subsection.

8.3.4 Quantum non-demolition measurements

Consider a generic harmonic oscillator, with mass m and frequency ω_0, described classically by a coordinate $x(t)$. The solution of the equation of motion with the initial conditions $x(0) = x_0$ and $\dot{x}(0) = v_0$ is

$$x(t) = x_0 \cos\omega_0 t + \frac{v_0}{\omega_0} \sin\omega_0 t\,. \tag{8.166}$$

Let $v(t) = \dot{x}(t)$, and define X_1, X_2 as

$$X_1 = x(t)\cos\omega_0 t - \frac{v(t)}{\omega_0}\sin\omega_0 t\,, \tag{8.167}$$

$$X_2 = x(t)\sin\omega_0 t + \frac{v(t)}{\omega_0}\cos\omega_0 t\,. \tag{8.168}$$

Using eq. (8.166) and the corresponding expression for $v(t)$, we see that $X_1 = x_0$ and $X_2 = v_0/\omega_0$, so X_1, X_2 are conserved on the equations of motion, and eq. (8.166) can be rewritten as

$$x(t) = {\rm Re}\left[(X_1 + iX_2)e^{-i\omega_0 t}\right]\,. \tag{8.169}$$

At the quantum level, we denote the operators by a caret, so $\hat{x}$ and $\hat{p}$ are the position and momentum operators, with $[\hat{x}, \hat{p}] = i\hbar$. As usual, the Hamiltonian of the harmonic oscillator is

$$\hat{H}_0 = \frac{\hat{p}^2}{2m} + \frac{1}{2}m\omega_0^2\hat{x}^2 = \hbar\omega_0\left(\hat{N} + \frac{1}{2}\right)\,, \tag{8.170}$$

where $\hat{N} = \hat{a}^\dagger\hat{a}$, and

$$\hat{a} = \left(\frac{m\omega_0}{2\hbar}\right)^{1/2}\left(\hat{x} + i\frac{\hat{p}}{m\omega_0}\right)\,, \tag{8.171}$$

$$\hat{a}^\dagger = \left(\frac{m\omega_0}{2\hbar}\right)^{1/2}\left(\hat{x} - i\frac{\hat{p}}{m\omega_0}\right)\,. \tag{8.172}$$

In the Heisenberg picture we define the operators $\hat{X}_1$ and $\hat{X}_2$ as in eqs. (8.167) and (8.168),

$$\hat{X}_1(t) = \hat{x}(t)\cos\omega_0 t - \frac{\hat{p}(t)}{m\omega_0}\sin\omega_0 t\,, \tag{8.173}$$

$$\hat{X}_2(t) = \hat{x}(t)\sin\omega_0 t + \frac{\hat{p}(t)}{m\omega_0}\cos\omega_0 t\,. \tag{8.174}$$

Similarly to what happens classically, in the absence of external forces the Heisenberg operators $\hat{X}_1(t)$ and $\hat{X}_2(t)$ are conserved,

$$\frac{d\hat{X}_i}{dt} = \frac{\partial\hat{X}_i}{\partial t} - \frac{i}{\hbar}[\hat{X}_i, H_0] = 0\,. \tag{8.175}$$

This property selects $\hat{X}_1$ and $\hat{X}_2$ as particularly useful observables, since any change they experience must be due to external disturbances, such as GWs or other external forces. The interaction of the quantum harmonic oscillator with an external classical force $F(t)$ can be described by an interaction Hamiltonian $\hat{H}_{\rm int} = -F(t)\hat{x}$. In the presence of $F(t)$, $\hat{X}_1$ and $\hat{X}_2$ are no longer conserved; rather

$$\frac{d\hat{X}_1}{dt} = -\frac{i}{\hbar}[\hat{X}_1, H_{\rm int}] = -\frac{F(t)}{m\omega_0}\sin\omega_0 t\,, \tag{8.176}$$

$$\frac{d\hat{X}_2}{dt} = -\frac{i}{\hbar}[\hat{X}_2, H_{\rm int}] = +\frac{F(t)}{m\omega_0}\cos\omega_0 t\,. \tag{8.177}$$

This integrates to

$$\hat{X}_1(t) = \hat{X}_1(t_0) - \frac{1}{m\omega_0}\int_{t_0}^{t} dt'\, F(t')\sin\omega_0 t'\,, \tag{8.178}$$

and similarly for $\hat{X}_2$. The important point is that, since $F(t)$ is a classical force, the second term on the right-hand side is a c-number rather than an operator. Suppose that at time t_0 we perform a measurement of the observable $\hat{X}_1$ on the oscillator. We will find some value X_1^0, and the measurement leaves the oscillator in the corresponding eigenstate $|X_1^0\rangle$ of $\hat{X}_1(t_0)$. In the Heisenberg picture the state $|X_1^0\rangle$ does not evolve, while the operator $\hat{X}_1(t)$ evolves as in eq. (8.178). Then, since the second term on the right-hand side of eq. (8.178) is a c-number, for $t > t_0$ we have

$$\hat{X}_1(t)|X_1^0\rangle = X_1(t)|X_1^0\rangle\,, \tag{8.179}$$

with

$$X_1(t) = X_1^0 - \frac{1}{m\omega_0}\int_{t_0}^{t} dt'\, F(t')\sin\omega_0 t'\,. \tag{8.180}$$

So, at time $t > t_0$ the oscillator is still in an eigenstate of $\hat{X}_1(t)$, and a measurement of $\hat{X}_1$ at time t will give the above value, and will not affect the oscillator state (apart possibly for a phase, since states in the Fock space that differ by a phase correspond to the same physical state). In other words, when the classical force $F(t)$ is acting, after the first measurement, all successive measurements of $\hat{X}_1$ leave unchanged the state of the oscillator, even if the result $X_1(t)$ of this measurement changes continuously in time, see eq. (8.180).

This is of course very different from what happens when we rather measure the position operator $\hat{x}(t)$ of the oscillator, since in this case each time we perform a measurement of $\hat{x}(t)$ we have a wavefunction reduction which forces the oscillator in an eigenstate of $\hat{x}(t)$, and the result obtained at $t = t_0$ does not fix uniquely the outcome of a successive measurement at $t > t_0$. It is clear that X_1 (or X_2) are the best quantities to be measured when quantum mechanics becomes important, since from a series of repeated measurements of it we can reconstruct deterministically the time-evolution of the external classical force $F(t)$. A measurement that leaves the state of the system unchanged, as the measurement of $\hat{X}_1(t)$ described above, is called a *quantum non-demolition* measurement.

Having established that $\hat{X}_1$ and $\hat{X}_2$ are the most useful observables for our purposes, we can discuss what the uncertainty principles has to tell about their measurement. From the definition, eq. (8.173), we see that

$$[X_1, X_2] = \frac{i\hbar}{m\omega_0}\,. \tag{8.181}$$

Therefore, on any state,

$$\Delta X_1 \Delta X_2 \geqslant \frac{1}{2}\,|\,\langle[X_1, X_2]\rangle\,| = \frac{\hbar}{2m\omega_0}\,. \tag{8.182}$$

Suppose that we measure X_1 and X_2 using an amplifier with a bandwidth $\Delta f \ll f_0$. This means that we sample the oscillator position over a time Δt much longer than the period of the oscillator. Therefore we are actually measuring the average value of X_1 and X_2 over a period, that we denote by $\bar{X}_1$ and $\bar{X}_2$, respectively. If we use a linear amplifier, when the input is given by eq. (8.169), the output is of the form

$$y(t) = \mathrm{Re}\,\left[A(\bar{X}_1 + i\bar{X}_2)e^{-i\omega_0 t}\right]\,, \tag{8.183}$$

with A a constant amplification factor, in general complex. Since $\bar{X}_1$ and $\bar{X}_2$ are treated symmetrically in this expression, their errors are equal, $\Delta\bar{X}_1 = \Delta\bar{X}_2$. In this case eq. (8.182) gives

$$\Delta\bar{X}_1 = \Delta\bar{X}_2 \geqslant \left(\frac{\hbar}{2m\omega_0}\right)^{1/2}\,. \tag{8.184}$$

Recall from eq. (8.173) that (X_1, X_2) are obtained from $(x, p/m\omega_0)$ performing a rotation by an angle $\omega_0 t$. Then $\Delta\bar{X}_1 = \Delta\bar{X}_2$ implies also $\Delta x = \Delta p/m\omega_0$ which, together with $\Delta x\Delta p \geqslant \hbar/2$, means

$$\Delta x = \frac{\Delta p}{m\omega_0} \geqslant \left(\frac{\hbar}{2m\omega_0}\right)^{1/2}\,. \tag{8.185}$$

Therefore, if we monitor the fundamental mode of the bar with a linear amplifier, quantum mechanics sets a limit to the error Δx. Writing, as

usual, $m = M/2$, where M is the total mass of the bar, we have

$$(\Delta x)_{\min} \simeq 2.9 \times 10^{-19}\,\mathrm{cm} \left(\frac{2000\,\mathrm{kg}}{M}\right)^{1/2} \left(\frac{1\,\mathrm{kHz}}{f_0}\right)^{1/2} . \tag{8.186}$$

In terms of energy, writing

$$\hat{H}_0 = \frac{m\omega_0^2}{2}\left[\left(\frac{\hat{p}}{m\omega_0}\right)^2 + \hat{x}^2\right] , \tag{8.187}$$

we see from eq. (8.185) that, even if the oscillator is in its ground state, there is a minimum error on the energy

$$(\Delta E)_{\min} \simeq \frac{m\omega_0^2}{2}\left[\left(\frac{\Delta p}{m\omega_0}\right)^2 + (\Delta x)^2\right] = \frac{1}{2}\hbar\omega_0 . \tag{8.188}$$

More generally, if one takes as wavefunction a Gaussian both in X_1 and X_2, centered on the expectation values $\langle\hat{X}_1\rangle$ and $\langle\hat{X}_2\rangle$, and with variances $\Delta X_1 = \Delta X_2 = (\hbar/2m\omega_0)^{1/2}$, one finds that the variance of the average number of quanta in this state is $\Delta N = (N + 1/4)^{1/2}$ and therefore

$$(\Delta E)_{\min} = \hbar\omega_0 \left(N + \frac{1}{4}\right)^{1/2} . \tag{8.189}$$

We have therefore understood how eq. (8.164) comes out: it is a consequence of the uncertainty principle *and* of the specific way of performing the measurement with a linear amplifier, which gives $\Delta X_1 = \Delta X_2$. Now, however, we can also understand how, at least in principle, such a limit can be evaded: from eq. (8.178) we see that measuring *either* X_1 *or* X_2 is sufficient to reconstruct to external force $F(t)$, which in our case means to measure the incoming GW. So, we need to perform a very precise measurement of, say, X_1, giving up completely the information of X_2. Strategies of this type are called back-action evasion measurements, since the back-action force on X_1 caused by the measurement process, which in general is responsible for the uncertainty principle, has been evaded, or rather has been concentrated uniquely on the conjugate variable X_2.

More precisely, from eq. (8.180), we have

$$\frac{dX_1(t)}{dt} = -\frac{1}{m\omega_0} F(t)\sin\omega_0 t , \tag{8.190}$$

and from this we can accurately reconstruct $F(t)$, except when $\sin\omega_0 t$ is close to zero. However, when $F(t)$ is a classical force, we can also use a second transducer, on which we measure only $X_2(t)$, since this second transducer is affected by the same classical force $F(t)$. Then from this measurement we get

$$\frac{dX_2(t)}{dt} = \frac{1}{m\omega_0} F(t)\cos\omega_0 t , \tag{8.191}$$

and $F(t)$ can be completely reconstructed.

8.3.5 Experimental sensitivities

In this section we discuss the sensitivities of existing resonant detectors. Actually, the experimental situation is in continuous evolution; all detectors typically alternate data-taking periods with upgrades, old experiments terminate their activity, and new ones are sometime proposed. Thus, any discussion of the experimental situation is bound to become obsolete on a relatively short time-scale. We therefore discuss only very briefly the various detectors, referring the reader to the web pages of the various collaborations in the Further Reading section for updated information, and we rather discuss what results can be achieved with existing or foreseeable sensitivities.

Presently (2007) three resonant bars are in operation: AURIGA (Legnaro, near Padua), EXPLORER (CERN) and NAUTILUS (Frascati, near Rome), while a fourth bar, ALLEGRO (Baton Rouge, Louisiana), terminated operation during 2007. EXPLORER and NAUTILUS are operated by the same collaboration (ROG). We show in Fig. 8.14 a picture of NAUTILUS and in Fig. 8.15 a picture of AURIGA. In Fig. 8.16 we show a typical strain sensitivity curve of the EXPLORER and NAUTILUS detector, and in Fig. 8.17 a typical the strain sensitivity of AURIGA. We see that, thanks to the improvement in the read-out system discussed in Section 8.2.2, this strain sensitivity has a minimum value

$$S_n^{1/2} \simeq 1 \times 10^{-21}\,\mathrm{Hz}^{-1/2} , \tag{8.192}$$

and stays below $4 \times 10^{-21}\,\mathrm{Hz}^{-1/2}$ over a bandwidth of 100 Hz. We now discuss, using the results of Section 7.3, the sensitivity to bursts, periodic and stochastic signals that can be obtained with these strain sensitivities.

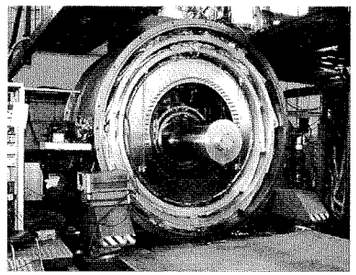

Fig. 8.14 A picture of the NAUTILUS resonant bar and of the cryostat.

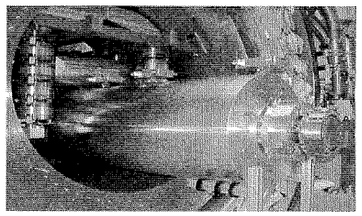

Fig. 8.15 A picture of the AURIGA resonant bar. The transducer is visible.

Sensitivity to bursts

Using eq. (7.96) at $S/N = 1$ (of course a higher threshold, typically of order 5–6, must be used), we can estimate that $|\tilde{h}(f_0)| \simeq [S_n/(4\Delta f)]^{1/2}$. Using an average reference value $S_n^{1/2} \sim 4 \times 10^{-21}\,\mathrm{Hz}^{-1/2}$ over a bandwidth $\Delta f \sim 100$ Hz gives the order-of magnitude estimate for the minimum detectable value of $\tilde{h}(f_0)$,

$$|\tilde{h}(f_0)| \sim 2 \times 10^{-22}\,\mathrm{Hz}^{-1} . \tag{8.193}$$

Assuming a sine-Gaussian waveform (7.103), centered on the resonance frequency f_0 of the detector and of duration τ_g, and using eq. (7.105), we get the minimum detectable value of the GW amplitude,

$$h_0 \sim 2 \times 10^{-19} \left(\frac{1\,\mathrm{ms}}{\tau_g}\right) , \tag{8.194}$$

or equivalently, using eq. (7.110), the minimum detectable value of h_{rss},

$$h_{\mathrm{rss}} \sim 5 \times 10^{-21}\,\mathrm{Hz}^{-1/2} \left(\frac{1\,\mathrm{ms}}{\tau_g}\right)^{1/2} . \tag{8.195}$$

[30] These are the values for NAUTILUS, but they are very close for the other bars.

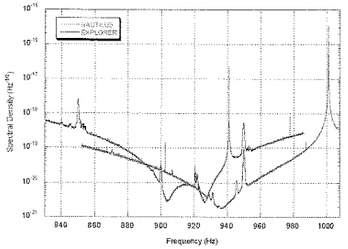

Fig. 8.16 The strain sensitivity $[S_n(f)]^{1/2}$ of EXPLORER (the curve with two minima) and NAUTILUS (the curve with one broad minimum) in 2004. The peaks around 940 and 1000 Hz, respectively, are reference signals sent to the detectors to monitor the SQUID gain.

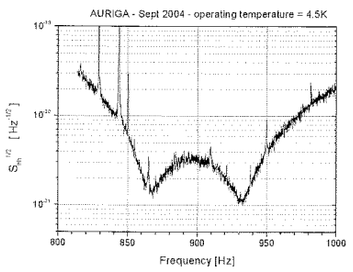

Fig. 8.17 The strain sensitivity $[S_n(f)]^{1/2}$ of AURIGA in 2004.

For resonant bars it is often useful to think directly in terms of the energy deposited by a burst in the detector. In this case, inserting the numerical values[30] $M = 2260$ kg, $L = 3$ m, $f_0 = 940$ Hz, and measuring E_s in milliKelvin, eq. (8.19) gives

$$\tilde{h}(f_0) \simeq 2.5 \times 10^{-22}\,\mathrm{Hz}^{-1} \left(\frac{E_s}{1\,\mathrm{mK}}\right)^{1/2} , \tag{8.196}$$

and we see from eq. (8.193) that present resonant detectors can measure excitations that leave in a bar an energy $E_s \sim 1$ mK. Assuming again a sine-Gaussian waveform centered within the detector bandwidth, and using eqs. (7.104) and (7.110), we get $h^2_{\rm rss} = (2/\pi)^{1/2}|\tilde{h}(f_0)|^2/\tau_g$. Inserting this into eq. (7.112) and using eq. (8.196) we find that a GW burst that deposited in a resonant bar an energy E_s should originate from a process that liberated in GWs the energy

$$\boxed{\Delta E_{\rm rad} \simeq 5 \times 10^{-5} M_\odot c^2 \left(\frac{E_s}{1\,\mathrm{mK}}\right) \left(\frac{r}{8\,\mathrm{kpc}}\right)^2 \left(\frac{1\,\mathrm{ms}}{\tau_g}\right) \left(\frac{f_0}{1\,\mathrm{kHz}}\right)^2 .} \tag{8.197}$$

The above equation tells us at what maximum distance a resonant bar can see a GW burst, given the minimum value of E_s that can be measured. For a GW burst that liberates an energy $10^{-2} M_\odot c^2$ (such as the merging phase of a NS-NS coalescence), with $f_0 = 1$ kHz and $\tau_g = 1$ ms, we get

$$r_{\rm max} \sim O(100)\,\mathrm{kpc} \left(\frac{1\,\mathrm{mK}}{E_{s,\rm min}}\right)^{1/2} , \tag{8.198}$$

so we have access to galactic events and to our immediate galactic neighborhood. However, events liberating $10^{-2} M_\odot c^2$ are extremely rare on a galactic scale. Less energetic events will be more common, but of course we can see them only if they are even closer. From eq. (8.197), setting $E_{s,\rm min} = 1$ mK, we see that for a phenomenon taking place at 80 pc (corresponding to the distance to the closest known neutron stars, while the closest estimated neutron star should be at 5–10 pc), we need a process that liberates $\Delta E_{\rm rad} \simeq 5 \times 10^{-9} M_\odot c^2$.

Sensitivity to periodic signals

The minimum detectable amplitude of a periodic signal has been computed in eq. (7.164). For present resonant bars, we normalize the spectral sensitivity to the value given in eq. (8.192). Recall also that $\eta = (S/N)\,\mathcal{N}^{1/4}\,\langle F_+^2\rangle^{-1/2}$, see eq. (7.165), is a factor that takes into account the desired level of S/N, the need to split the data into $\mathcal{N}$ stack for computational feasibility, and the angular efficiency factor $\langle F_+^2\rangle^{-1/2}$. For resonant bars $\langle F_+^2\rangle^{-1/2} = (15/4)^{1/2} \simeq 2$, see Table 7.1. For a blind full sky search one could use stacks of length less than one hour, which is about the maximum value for which the Doppler effect within a stack can be neglected, see eq. (7.140). This, for one year of data, gives $\mathcal{N} \sim 10^4$, so $\mathcal{N}^{1/4} \simeq 10$. Therefore, at $S/N = 1$, we have $\eta \simeq 20$.

Using this reference values for η, the minimum detectable amplitude of a periodic signal, eq. (7.164), can be rewritten as

$$h_{\rm min} = 4 \times 10^{-24} \left(\frac{\eta}{20}\right) \left(\frac{S_n^{1/2}(f_0)}{10^{-21}\,\mathrm{Hz}^{-1/2}}\right) \left(\frac{3 \times 10^7\,\mathrm{s}}{T}\right)^{1/2} , \tag{8.199}$$

and, using eq. (7.166), the maximum distance at which we can see the signal from a spinning NS is

$$r \simeq 290\,\mathrm{pc} \left(\frac{20}{\eta}\right) \left(\frac{10^{-21}\,\mathrm{Hz}^{-1/2}}{S_n^{1/2}(f_0)}\right) \left(\frac{T}{3 \times 10^7\,\mathrm{s}}\right)^{1/2} \times \left(\frac{\epsilon}{10^{-6}}\right) \left(\frac{I_{zz}}{10^{38}\,\mathrm{kg\,m^2}}\right) \left(\frac{f_0}{1\,\mathrm{kHz}}\right)^2 . \tag{8.200}$$

However, if one is targeting a specific pulsar, the reference values for $S_n^{1/2}$ and η change. First of all, as discussed in Section 7.6, the need to divide the observation time into $\mathcal{N}$ stacks with $\mathcal{N} \gg 1$ emerges only when we perform blind searches, in order to keep the computational burden within affordable limits. In a dedicated search to a single source there is no need for it, and the only limitation comes from the maximum consecutive time that a detector can run without interruptions due to maintenance. Taking $T_{\rm stack} \sim 1 - 2$ week, in one year we get $\mathcal{N}^{1/4} \sim 2.5$ and therefore, at $S/N = 1$, we can take $\eta = 5$ as a more appropriate reference value.

Furthermore, if we know the frequency of the source, we can tune the frequency of the detector to this value.[31] Once one of the resonance frequencies of the bar–transducer system has been tuned to the target source, we can give up the condition of having a bandwidth as large as possible, in favor of a better sensitivity at the resonance frequency. According to the discussion in Section 8.3, this means that we must reduce as much as possible the thermal noise, so that it goes below the amplifier noise, which is by itself very much suppressed at the resonance frequencies $f_\pm$. In this way, better peak sensitivity can indeed by obtained. For instance, AURIGA reached $S_n^{1/2} = 4 \times 10^{-22}\,\mathrm{Hz}^{-1/2}$ over a 2 Hz bandwidth, cooling the detector down to 0.24 K . Using these reference values for $S_n^{1/2}$ and η, eqs. (8.199) and (8.200) can be rewritten as

$$h_{\rm min} = 4 \times 10^{-25} \left(\frac{\eta}{5}\right) \left(\frac{S_n^{1/2}(f_0)}{4 \times 10^{-22}\,\mathrm{Hz}^{-1/2}}\right) \left(\frac{3 \times 10^7\,\mathrm{s}}{T}\right)^{1/2} , \tag{8.201}$$

$$r \simeq 2.9\,\mathrm{kpc} \left(\frac{5}{\eta}\right) \left(\frac{4 \times 10^{-22}\,\mathrm{Hz}^{-1/2}}{S_n^{1/2}(f_0)}\right) \left(\frac{T}{3 \times 10^7\,\mathrm{s}}\right)^{1/2} \times \left(\frac{\epsilon}{10^{-6}}\right) \left(\frac{I_{zz}}{10^{38}\,\mathrm{kg\,m^2}}\right) \left(\frac{f_0}{1\,\mathrm{kHz}}\right)^2 . \tag{8.202}$$

[31] Within $O(50)$ Hz this can be done simply at the level of electronics, changing the electric field in the transducer, which results in a change in the normal modes of the three-modes system made by the two mechanical oscillator and the electric mode. Otherwise, if one has a specific target in mind, one could build a dedicated bar, choosing length and material so to have the appropriate resonance frequency.

Coalescences

This is the kind of source for which the difference between bars and interferometers is more important. A ground-based interferometer is a broad-band detector, that operates from a few tens of Hz to a few kHz. In this bandwidth, we saw in Sections 4.1 and 7.7.2 that we can follow the evolution of the waveform for a number of cycles $\mathcal{N}_c \sim 10^4$, which results in a gain of order $\mathcal{N}_c^{1/2} \sim 100$ in the maximum distance at which we can detect a coalescence. For resonant detectors this is not possible. First of all, for BH-BH binaries with typical BH masses $\sim 10 M_\odot$, the coalescence takes place when $f_{\rm gw} \sim 400$ Hz, see eq. (4.40), therefore the signal never enters in the bandwidth of resonant bars, which operate at the kHz.[32] For NS-NS binaries the coalescence takes place at the kHz, but then the bars only see the final merging phase, which lasts a few milliseconds, rather than the long inspiral phase. Thus, for a bar, a NS-NS coalescence is just a burst, and there is no gain associated to the number of cycles $\mathcal{N}_c$.

[32] To build a resonant detector with a lower resonance frequency one should increase its size and mass, with a corresponding increase in technical difficulties, particularly in the cryogeny, and in the financial costs.

Stochastic backgrounds

Performing the correlation between two resonant bars, both working in a relatively narrow bandwidth around a frequency f_0, the expression of the signal-to-noise ratio for stochastic backgrounds, eq. (7.239), becomes

$$\frac{S}{N} \simeq (2T\Delta f)^{1/2} \Gamma(f_0) \frac{S_h(f_0)}{S_n(f_0)} , \tag{8.203}$$

and for two resonant bars $\Gamma(f) = (8/15)\gamma(f)$, see eqs. (7.228) and (7.37) and Table 7.1 Therefore the minimum detectable value of $S_h(f_0)$, using an optimistic value $S/N = 1$, is

$$S_h^{1/2}(f_0) \simeq 7 \times 10^{-24}\,{\rm Hz}^{-1/2} \left(\frac{25\,{\rm Hz}}{\Delta f}\right)^{1/4} \left(\frac{1\,{\rm yr}}{T}\right)^{1/4} \times \left(\frac{S_n^{1/2}(f_0)}{10^{-21}\,{\rm Hz}^{-1/2}}\right) \left(\frac{1}{\gamma(f_0)}\right)^{1/2} , \tag{8.204}$$

corresponding to

$$h_0^2 \Omega_{\rm gw}(f_0) \simeq 6 \times 10^{-2} \left(\frac{f_0}{1\,{\rm kHz}}\right)^3 \left(\frac{25\,{\rm Hz}}{\Delta f}\right)^{1/2} \left(\frac{1\,{\rm yr}}{T}\right)^{1/2} \times \left(\frac{S_n^{1/2}(f_0)}{10^{-21}\,{\rm Hz}^{-1/2}}\right)^2 \frac{1}{\gamma(f_0)} . \tag{8.205}$$

As we will discuss in Vol. 2, there are bounds on stochastic background of GWs of cosmological origin that forbid values of $h_0^2\Omega_{\rm gw}$ larger than $\sim 10^{-5}$–10^{-6} at any frequency, and astrophysical backgrounds are also expected to be below this value. With these sensitivities, resonant bars do not seem therefore capable of detecting a stochastic background, and for this reason these searches have not been much pursued.

The sensitivity at the quantum limit

We have seen in the previous sections that present resonant bars are dominated by thermal and read-out noise. Thermal noise in principle can be lowered cooling further the bars and increasing the quality factors, while for the read-out noise we have seen that an intrinsic limitation, if we do not use quantum non-demolition techniques, is given by the quantum limit.

We first of all compute under what conditions the thermal noise can be reduced below the quantum limit. Combining eqs. (7.96) and (8.19) we get

$$S_n(f_0) \simeq 4\Delta f \, \frac{E_s}{16 M L^2 f_0^4} . \tag{8.206}$$

If the read-out noise allows us to detect a vibration corresponding to N phonons, $S_n^{\rm ampl}(f_0)$ is obtained from eq. (8.206) setting $E_s = N\hbar\omega_0$. We express L in terms of the speed of sound, $L = \pi v_s/\omega_0$, and we obtain

$$S_n^{\rm ampl}(f_0) \simeq \frac{2\pi}{M v_s^2} \left(\frac{\Delta f}{f_0}\right) N\hbar . \tag{8.207}$$

As for thermal noise, eq. (8.137) gives

$$S_n^{\rm thermal}(f_0) = \frac{\pi}{Q} \frac{kT}{M v_s^2} \frac{1}{f_0} . \tag{8.208}$$

Requiring that $S_n^{\rm thermal}(f_0) < S_n^{\rm ampl}(f_0)$ we therefore get

$$\boxed{Q > \frac{kT}{2N\hbar\Delta f} .} \tag{8.209}$$

The quantum limit corresponds to $N = 1$, and we then find that, to bring thermal noise below the quantum limit, we need

$$Q > 6.6 \times 10^7 \left(\frac{T}{100\,{\rm mK}}\right) \left(\frac{100\,{\rm Hz}}{\Delta f}\right) . \tag{8.210}$$

Therefore, for a detector cooled at $T = 20$ mK and with a bandwidth $\Delta f = 100$ Hz, we need $Q > 10^7$. This is not an unrealistic target with present improvements in materials. Of course, beside being able to push thermal noise below the quantum limit, we must also be able to detect excitations with $N = O(1)$ in a two-ton bar. Presently, using double SQUIDs, one is able to reach $N = O(100)$, and further progress can be expected in the near future. It therefore appears that reaching the quantum limit, or at least getting close to it, is a challenging but not unrealistic target, and we can take the quantum limit as the estimate of the best sensitivity that resonant-mass detectors could achieve with improvements of existing technologies.[33]

Numerically, taking $M = 2300$ kg, $v_s = 5400$ m/s, $\Delta f/f_0 \simeq 0.1$, and setting $N = 1$, eq. (8.207) gives

$$\boxed{\left[S_n^{1/2}(f_0)\right]_{\rm quantum\ limit} \sim 3 \times 10^{-23}\,{\rm Hz}^{-1/2} .} \tag{8.211}$$

[33] This is not necessarily the ultimate sensitivity of resonant detectors, since, as discussed in Section 8.3.4, in principle the quantum limit can be circumvented using quantum non-demolition techniques.

For periodic signals, the minimum GW amplitude that can be detected with such a strain sensitivity, when one searches for a specific target, can be read from eq. (8.201), and we see that it is

$$h_{\rm min} = 3 \times 10^{-26} \left(\frac{\eta}{5}\right) \left(\frac{3 \times 10^7\,{\rm s}}{T}\right)^{1/2} , \tag{8.212}$$

corresponding to a maximum distance at which a spinning NS is visible

$$r \simeq 40\,{\rm kpc} \left(\frac{5}{\eta}\right) \left(\frac{T}{3 \times 10^7\,{\rm s}}\right)^{1/2} \left(\frac{\epsilon}{10^{-6}}\right) \left(\frac{I_{zz}}{10^{38}\,{\rm kg\,m^2}}\right) \left(\frac{f_0}{1\,{\rm kHz}}\right)^2 . \tag{8.213}$$

Concerning bursts, detecting a single quantum at $f_0 = 900$ Hz means to measure an energy $E_s = 4 \times 10^{-5}$ mK. From eq. (8.198) we see that, with this sensitivity, we can measure a burst which releases 10^{-2} solar masses, such as a NS-NS coalescence, up to about 15 Mpc, which is just the distance to the Virgo cluster. However, recalling that these estimates assumed $S/N = 1$ we see that, even at the quantum limit, we would not really have access to the Virgo cluster, but rather to distances of order a few Mpc. To explore larger distances with a resonant bar, it would be necessary to use quantum non-demolition techniques to circumvent the quantum limit, as discussed in Section 8.3.4.

In terms of the dimensionless GW amplitude h_0 for a burst with duration $\tau_g = 1$ ms, with the above sensitivity eq. (8.194) is replaced by $h_0 \sim 2 \times 10^{-21}$. The same result can be obtained, in a physically transparent way, simply applying the uncertainty principle to the harmonic oscillator ξ_0 that represents the bar's fundamental mode. From eq. (8.29) we see that the maximum amplitude ξ_0 of the bar oscillation is

$$\Delta\xi_0 = \frac{2L}{\pi^2}\, h_0 \omega_0 \tau_{\rm g} . \tag{8.214}$$

On the other hand, for any harmonic oscillator of mass m, if we sense its motion without using quantum non-demolition techniques, we have $\Delta p = m\omega_0 \Delta x$, and then the uncertainty principle $\Delta x \Delta p \geqslant \hbar$ implies

$$\Delta x \geqslant \sqrt{\frac{\hbar}{m\omega_0}} . \tag{8.215}$$

Applying this to the oscillator described by ξ_0, and recalling that its effective mass is $m = M/2$, where M is the mass of the bar, we get

$$\frac{2L}{\pi^2}\, h_0 \omega_0 \tau_{\rm g} \geqslant \sqrt{\frac{2\hbar}{M\omega_0}} \tag{8.216}$$

and therefore, for a burst with duration $\tau_{\rm g}$ such that $f_0 \tau_{\rm g} \simeq 1$,

$$h_0 \geqslant \left(\frac{\pi}{2\sqrt{2}}\right) \frac{1}{L} \sqrt{\frac{\hbar}{M\omega_0}} \simeq \frac{1}{L} \sqrt{\frac{\hbar}{M\omega_0}} . \tag{8.217}$$

Taking $M = 2300$ kg and $L = 3$ m, this gives $h_0 \gtrsim 1 \times 10^{-21}$, in agreement with the previous estimate.

8.4 Resonant spheres

We conclude this chapter with a discussion of spherical resonant-mass detectors. From a conceptual point of view, this study reveals interesting features of the interaction of GWs with a macroscopic body. In particular we will see that, due to the spin-2 nature of the gravitational field, GWs couple only to some quadrupolar normal modes of the sphere and, more generally, a spin-s field couples only to some normal modes with angular dependence given by the spherical harmonics Y_{lm} with $l = s$. From the experimental point of view, we will see that resonant spheres can improve on resonant bars on at least three aspects. First, for a given resonance frequency, they are more massive, and therefore have a larger cross-section for absorption of GWs, and hence a better sensitivity. Second, a sphere has isotropic sensitivity and offers a full sky coverage, while all other detectors have blind directions. And third, using the information in the different quadrupolar modes of the sphere, it is possible to reconstruct the arrival direction and the polarization of a GW, something that cannot be done with a single bar or interferometer.

8.4.1 The interaction of a sphere with GWs

The three-dimensional equations of elasticity

In Section 8.1 we studied the response to GWs of a cylindrical bar, treating the problem as one-dimensional. To study a resonant sphere, instead, we need the full equations of elasticity in a three-dimensional body, which we recall in this section.[34] We first write the equations for a generic elastic body, and we will later specialize to a sphere.

We consider an infinitesimal volume element of the elastic body, located at the position $\mathbf{x}$. Under the action of an external force, like that exerted by a GW, it will be displaced to a new position $\mathbf{x} + \mathbf{u}(\mathbf{x}, t)$. Within elasticity theory the equation governing the dynamics of $\mathbf{u}(\mathbf{x}, t)$ is

$$\rho \frac{\partial^2 u_i}{\partial t^2} = \frac{\partial \sigma_{ij}}{\partial x^j} + f_i , \tag{8.218}$$

where $\boldsymbol{f}$ is the force per unit volume acting on the elastic body, and σ_{ij} is called the stress tensor. Hooke's law states that, for homogeneous and isotropic media,

$$\sigma_{ij} = \lambda u_{kk}\, \delta_{ij} + 2\mu\, u_{ij} , \tag{8.219}$$

where $u_{lm} \equiv (1/2)(\partial_l u_m + \partial_m u_l)$ and λ and μ are known as the Lamé coefficients.[35] The equation of motion (8.218) then becomes

$$\rho \frac{\partial^2 \mathbf{u}}{\partial t^2} = (\lambda + \mu) \boldsymbol{\nabla}(\boldsymbol{\nabla} \cdot \mathbf{u}) + \mu \nabla^2 \mathbf{u} + \boldsymbol{f} . \tag{8.223}$$

The boundary condition (in the absence of external tractions on the surface of the body) is that, on the surface, $\sigma_{ij} n_j = 0$, where $\hat{\mathbf{n}}$ is the unit normal to the surface of the elastic body. Using eq. (8.219) this can be rewritten as

$$\lambda(\boldsymbol{\nabla} \cdot \mathbf{u})\hat{\mathbf{n}} + 2\mu(\hat{\mathbf{n}} \cdot \boldsymbol{\nabla})\mathbf{u} + \mu \hat{\mathbf{n}} \times (\boldsymbol{\nabla} \times \mathbf{u}) = 0 . \tag{8.224}$$

[34] See, e.g. Landau and Lifshitz, Vol VII (1970) or Love (1944).

[35] Alternatively one can use the combinations Y (Young modulus) and σ_P (Poisson ratio), related to the Lamé coefficients by

$$\mu = \frac{Y}{2(1 + \sigma_P)} , \tag{8.220}$$

$$\lambda = \frac{\sigma_P Y}{(1 - 2\sigma_P)(1 + \sigma_P)} , \tag{8.221}$$

so in particular

$$\sigma_P = \frac{\lambda}{2(\mu + \lambda)} . \tag{8.222}$$

Typical materials have $\lambda/(2\mu)$ close to one. For instance the alloy Al 5056 used in many resonant detectors at cryogenic temperatures has $\lambda \simeq 6.3 \times 10^{10}{\rm N/m^2}$ and $\mu \simeq 3.0 \times 10^{10}{\rm N/m^2}$, so $\lambda/(2\mu) = 1.05$. Observe that for $\lambda/(2\mu) = 1$ we have $\sigma_P = 1/3$.

To search for the normal modes we set the external force $\boldsymbol{f} = 0$ and we write

$$\mathbf{u}(\mathbf{x}, t) = \mathbf{u}(\mathbf{x}, \omega) e^{-i\omega t} + c.c., \tag{8.225}$$

so $\mathbf{u}(\mathbf{x}, \omega)$ satisfies

$$(\lambda + \mu)\boldsymbol{\nabla}(\boldsymbol{\nabla} \cdot \mathbf{u}) + \mu \nabla^2 \mathbf{u} = -\rho\omega^2 \mathbf{u}\,. \tag{8.226}$$

To solve eq. (8.226) we separate $\mathbf{u}(\mathbf{x}, \omega)$ into its longitudinal and transverse parts, $\mathbf{u} = \mathbf{u}_\parallel + \mathbf{u}_\perp$, defined by $\boldsymbol{\nabla} \times \mathbf{u}_\parallel = 0$ and $\boldsymbol{\nabla} \cdot \mathbf{u}_\perp = 0$. Substituting this into (8.226) (and taking once the divergence and once the curl of the resulting equation) we get the two equations

$$(\nabla^2 + q^2)\mathbf{u}_\parallel(\mathbf{x}, \omega) = 0\,, \tag{8.227}$$

$$(\nabla^2 + k^2)\mathbf{u}_\perp(\mathbf{x}, \omega) = 0\,, \tag{8.228}$$

where $q^2 = \rho\omega^2/(\lambda + 2\mu)$ and $k^2 = \rho\omega^2/\mu$. Observe that k and q are related by

$$\frac{q^2}{k^2} = \frac{\mu}{\lambda + 2\mu}\,. \tag{8.229}$$

Equations (8.227) and (8.228) show that $\mathbf{u}_\parallel(\mathbf{x}, t)$ and $\mathbf{u}_\perp(\mathbf{x}, t)$ describe waves propagating with velocities $v_\parallel = [(\lambda+2\mu)/\rho]^{1/2}$ and $v_\perp = (\mu/\rho)^{1/2}$, respectively.[36] Writing $\mathbf{u}(\mathbf{x}, \omega)$ as a superposition of plane waves,

$$\mathbf{u}(\mathbf{x}, \omega) = \sum_{\mathbf{k}} \tilde{\mathbf{u}}(\mathbf{k}, \omega) e^{i\mathbf{k}\cdot\mathbf{x}}\,, \tag{8.230}$$

we see that for $\mathbf{u}_\parallel$ we have $\mathbf{k}\times\tilde{\mathbf{u}}(\mathbf{k}, \omega) = 0$, so it describes a wave which displaces a volume element of the material along its propagation direction $\hat{\mathbf{k}}$, i.e. a longitudinal wave, and similarly $\mathbf{u}_\perp$ displaces it in the transverse direction. Furthermore, the condition $\boldsymbol{\nabla}\cdot\mathbf{u}_\perp$ means that transverse waves do not involve changes in volume, contrary to $\mathbf{u}_\parallel$ which induces compressions and expansions of the volume element. We can construct the longitudinal and transverse solutions introducing two scalar functions $\chi(\mathbf{x}; q)$ and $\varphi(\mathbf{x}; k)$. We write the longitudinal part as

$$\mathbf{u}_\parallel(\mathbf{x}, \omega) = \boldsymbol{\nabla}\chi(\mathbf{x}, q)\,, \tag{8.231}$$

while, defining the operator $\mathbf{L} = -i\mathbf{r}\times\boldsymbol{\nabla}$, we can form two independent transverse vectors, that we denote by $\mathbf{u}_t(\mathbf{x}, \omega)$ and $\mathbf{u}_{t'}(\mathbf{x}, \omega)$, respectively,

$$\mathbf{u}_t(\mathbf{x}, \omega) = i\boldsymbol{\nabla} \times \mathbf{L}\varphi(\mathbf{x}, k) \qquad \mathbf{u}_{t'}(\mathbf{x}, \omega) = i\boldsymbol{L}\varphi(\mathbf{x}, k)\,. \tag{8.232}$$

Equations (8.227) and (8.228) become

$$(\nabla^2 + q^2)\chi(\mathbf{x}, q) = 0\,, \qquad (\nabla^2 + k^2)\varphi(\mathbf{x}, k) = 0\,. \tag{8.233}$$

The most general solution for $\mathbf{u}$ is therefore of the form

$$\begin{aligned}\mathbf{u}(\mathbf{x}, \omega) &= C_0\mathbf{u}_\parallel(\mathbf{x}, \omega) + C_1\mathbf{u}_t(\mathbf{x}, \omega) + C_2\mathbf{u}_{t'}(\mathbf{x}, \omega) \\ &= C_0\boldsymbol{\nabla}\chi(\mathbf{x}, q) + iC_1\boldsymbol{\nabla}\times\boldsymbol{L}\varphi(\mathbf{x}, k) + iC_2\boldsymbol{L}\varphi(\mathbf{x}, k)\,,\end{aligned} \tag{8.234}$$

[36] Observe that $v_\parallel$ is different from $v_s \equiv (Y/\rho)^{1/2}$ which, as we saw below eq. (8.1), is the longitudinal speed of sound in a thin bar, even if both velocities refer to longitudinal waves. The reason is that v_s is the velocity of longitudinal sound waves in the limit in which the transverse section of the bar is much smaller than the wavelength of the sound waves, while $v_\parallel$ is the velocity of longitudinal sound waves when the transverse dimension is at least as large as the wavelength.

where χ and φ are solutions of eq. (8.233). We now impose the boundary condition (8.224). This quantizes the allowed values of k (and therefore of q, since q and k are related by eq. (8.229)) and, apart from an overall normalization factor, fixes the value of the constants C_0, C_1 and C_2. The solutions so obtained are the normal modes of the system, and we denote them by $\boldsymbol{\psi}_N(\mathbf{x})$, where N labels collectively all the labels that are necessary to classify the normal modes. Since the normal modes form a complete set, the most general displacement $\mathbf{u}(\mathbf{x}, t)$ that satisfies the boundary conditions can be expanded as

$$\mathbf{u}(\mathbf{x}, t) = \sum_N \xi_N(t)\boldsymbol{\psi}_N(\mathbf{x})\,. \tag{8.235}$$

For a thin cylindrical bar the problem is one-dimensional, and we found in Section 8.1.1 that there are two families of normal modes, given by $\boldsymbol{\psi}_{n,1}(x) = \sin[\pi x(2n+1)/L]$ and $\boldsymbol{\psi}_{n,2}(x) = \cos[\pi x(2n+2)/L]$, so in this case $N = \{n, \alpha\}$ with $\alpha = 1, 2$ a discrete label. We also found that the modes $\boldsymbol{\psi}_{n,2}$ do not couple to GWs while the coupling of the modes $\boldsymbol{\psi}_{n,1}$ to GWs can be summarized in terms of an effective mass of the mode and an effective external force. In the next subsections we discuss the analogous results for a sphere.

The normal modes of a sphere

We can now specify the above general formalism to a spherical elastic body of radius R. The solution of eq. (8.233) is

$$\chi(\mathbf{x}, q) = j_l(qr)Y_{lm}(\theta, \phi)\,, \qquad \varphi(\mathbf{x}, k) = j_l(kr)Y_{lm}(\theta, \phi)\,, \tag{8.236}$$

where $j_l(z)$ is the spherical Bessel function. Inserting this into eq. (8.234) and imposing the boundary condition (8.224) we find two families of solutions, called toroidal and spheroidal modes. To write the result in a compact form, it is useful to define the functions

$$\beta_0(z) \equiv \frac{j_l(z)}{z^2}\,, \quad \beta_1(z) \equiv \frac{d}{dz}\left(\frac{j_l(z)}{z}\right)\,, \quad \beta_2(z) \equiv \frac{d^2}{dz^2}j_l(z)\,, \tag{8.237}$$

$$\beta_3(z) = \frac{1}{2}[\beta_2(z) + (l-1)(l+2)\beta_0(z)]\,, \tag{8.238}$$

$$\beta_4(z) = \beta_2(z) - \frac{\lambda}{2\mu}z^2\beta_0(z)\,. \tag{8.239}$$

Then we have the following classification.

Spheroidal modes. These modes have $l \geqslant 0$. When $l \neq 0$, their allowed values of k are the solutions of the equation

$$\beta_3(kR)\beta_4(qR) - l(l+1)\beta_1(kR)\beta_1(qR) = 0\,, \tag{8.240}$$

where q and k are related by eq. (8.229). For each l this equation has an infinity of solutions, that we denote by k^S_{nl}, with $n = 1, 2, \ldots$. Equa-

Table 8.1 The values of k^S_{nl} for $l = 0$ and $l = 2$ and $n = 1, \dots 4$, taking $\lambda/(2\mu) = 1.05$, which corresponds to the alloy Al 5056. (In a real detector, these values change by $O(10\%)$ because of the effect of the suspension system.)

l	n	$(kR)^S$	l	n	$(kR)^S$
0	1	5.580	2	1	2.651
	2	12.394		2	5.111
	3	18.870		3	8.639
	4	24.286		4	11.100

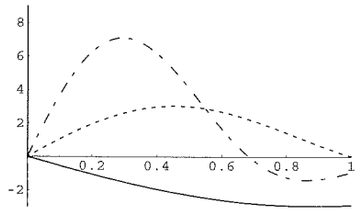

Fig. 8.18 The functions $a_{nl}(r)$, for $l = 2$ and $n = 1$ (solid line), $n = 2$ (dashed line), and $n = 3$ (dot-dashed), plotted against r/R, for $\lambda/(2\mu) = 1.05$. The functions $a_{nl}(r)$ are normalized according to eq. (8.246).

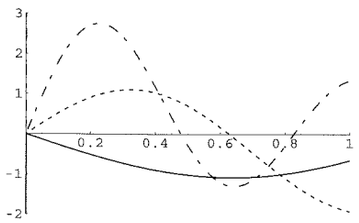

Fig. 8.19 The functions $b_{nl}(r)$, for $l = 2$ and $n = 1$ (solid line), $n = 2$ (dashed line), and $n = 3$ (dot-dashed), plotted against r/R, for $\lambda/(2\mu) = 1.05$. The functions b_{nl} are and normalized according to eq. (8.246).

tion (8.240) however does not depend on m, so there is a $(2l+1)$-fold degeneracy. The corresponding frequencies are obtained from eq. (8.228),

$$\boxed{\omega^S_{nl} = (\mu/\rho)^{1/2}\, k^S_{nl}\,.} \tag{8.241}$$

The explicit form of the spheroidal modes with $l \neq 0$ is

$$\boxed{\boldsymbol{\psi}^S_{nlm}(r,\theta,\phi) = [a_{nl}(r)\hat{\mathbf{r}} + b_{nl}(r)R\boldsymbol{\nabla}]\, Y_{lm}(\theta,\phi)\,,} \tag{8.242}$$

where

$$a_{nl}(r) = c_{nl}\left[\alpha_{nl}\frac{dj_l(z)}{dz}|_{z=q^S_{nl}r} - \beta_{nl}\; l(l+1)\frac{j_l(z)}{z}|_{z=k^S_{nl}r}\right], \tag{8.243}$$

$$b_{nl}(r) = c_{nl}\,\frac{r}{R}\left[\alpha_{nl}\frac{j_l(z)}{z}|_{z=q^S_{nl}r} - \beta_{nl}\left(\frac{j_l(z)}{z} + \frac{dj_l(z)}{dz}\right)|_{z=k^S_{nl}r}\right].$$

The constants α_{nl} and β_{nl} are given by

$$\alpha_{nl} = \beta_3(k^S_{nl}R)\,, \qquad \beta_{nl} = \frac{q}{k}\beta_1(q^S_{nl}R)\,. \tag{8.244}$$

The constants c_{nl} are normalization factors. We fix them requiring

$$\int_V d^3x\, \rho\, (\boldsymbol{\psi}^S_{nlm})^* \cdot \boldsymbol{\psi}^S_{nlm} = M\,, \tag{8.245}$$

where M is the mass of the sphere and V its volume. If ρ is constant, as will typically be the case, the normalization condition becomes

$$\int_V d^3x\, (\boldsymbol{\psi}^S_{nlm})^* \cdot \boldsymbol{\psi}^S_{nlm} = V\,. \tag{8.246}$$

We can also write eq. (8.242) in the equivalent form

$$\boldsymbol{\psi}^S_{nlm}(r,\theta,\phi) = A_{nl}(r)Y_{lm}(\theta,\phi)\hat{\mathbf{r}} - B_{nl}(r)\, i\hat{\mathbf{r}} \times \mathbf{L}Y_{lm}(\theta,\phi)\,, \tag{8.247}$$

where $A_{nl}(r) = a_{nl}(r)$ and $B_{nl}(r) = (R/r)b_{nl}(r)$. The functions $a_{nl}(r)$ and $b_{nl}(r)$ are plotted in Figs. 8.18 and 8.19.

For $l = 0$, instead, the allowed values of k are the solution of the equation

$$\beta_4(qR) = 0\,, \tag{8.248}$$

and the spheroidal modes are given by

$$\boldsymbol{\psi}^S_{n00}(r,\theta,\phi) = a_{n0}(r)\hat{\mathbf{r}}\,, \qquad a_{n0}(r) = c_{n0}\frac{dj_0}{dz}|_{z=q^S_{n0}r}\,. \tag{8.249}$$

Therefore the spheroidal modes with $l = 0$ are purely radial. In Table 8.1 we give the value of k^S_{nl} for some of the lowest $l = 0$ and $l = 2$ spheroidal modes, computed numerically from eqs. (8.240) and (8.248), taking $\lambda/(2\mu) = 1.05$ (as we will see in the next subsection, the modes $l = 2$ are the most interesting, since they are the only ones coupled to GWs). Observe that the numerical values of k^S_{nl} depend on $\lambda/(2\mu)$.

Toroidal modes. These modes are purely transverse and exist only for $l \geqslant 1$. The eigenvalues k^T_{nl} are determined by the equation $\beta_1(kR) = 0$ and have the form

$$\boldsymbol{\psi}^T_{nlm}(r,\theta,\phi) = c'_{nl}\, j_l(k^T_{nl}r) i\mathbf{L}Y_{lm}\,, \tag{8.250}$$

with c'_{nl} the normalization constant. Observe that $i\mathbf{L}Y_{lm} = \mathbf{r} \times \boldsymbol{\nabla}Y_{lm}$ is orthogonal both to $Y_{lm}\hat{\mathbf{r}}$ and to $\boldsymbol{\nabla}Y_{lm}$, i.e. to the displacements due to the spheroidal modes. The values of k^T_{nl} for $l = 1, 2$ and $n = 1, \dots, 4$ are given in Table 8.2. They are independent of $\lambda/(2\mu)$, since they are determined only by the function $\beta_1(z)$, given in eq. (8.237).

Table 8.2 The values of k^T_{nl} for $l = 1$ and $l = 2$, and $n = 1, \dots 4$. They do not depend on $\lambda/(2\mu)$.

l	n	$(kR)^T$	l	n	$(kR)^T$
1	1	5.763	2	1	2.501
	2	9.095		2	7.136
	3	12.323		3	10.515
	4	15.515		4	13.772

The interaction of the normal modes with GWs

We next discuss how these normal modes interact with GWs. We start from the expansion of the displacement $\mathbf{u}(\mathbf{x}, t)$ in terms of normal modes, eq. (8.235), and we substitute it into eq. (8.223). Using the fact that, by definition, the normal modes $\boldsymbol{\psi}_N(\mathbf{x})$ satisfy eq. (8.226) with $\omega = \omega_N$, we get

$$\rho\sum_{N'}(\ddot{\xi}_{N'} + \omega^2_{N'}\xi_{N'})\boldsymbol{\psi}_{N'}(\mathbf{x}) = \boldsymbol{f}\,. \tag{8.251}$$

Here $N = \{nlm;\alpha\}$, where the label $\alpha = \{S, T\}$ denotes spheroidal and toroidal modes, respectively. To obtain an equation for ξ_N we take the scalar product of both sides by $\boldsymbol{\psi}^*_N$ and we integrate over d^3x. Since the normal modes are orthogonal, and normalized as in eq. (8.245), we get

$$\ddot{\xi}_N + \omega^2_N\xi_N = \frac{1}{M}\int d^3x\, \boldsymbol{f}\cdot\boldsymbol{\psi}^*_N\,. \tag{8.252}$$

Recall that $\boldsymbol{f}$ is the force per unit volume. In the case of GWs, eq. (8.2) gives $f_i = (1/2)\ddot{h}^{TT}_{ij}x^j\rho$ and therefore (omitting for simplicity the label TT on h_{ij})

$$\boxed{\ddot{\xi}_N + \gamma_N\dot{\xi}_N + \omega^2_N\xi_N = \frac{1}{2V}\ddot{h}_{ij}\int_V d^3x\, (\boldsymbol{\psi}^*_N)^i x^j\,,} \tag{8.253}$$

where on the left-hand side we also added a term $\gamma_N\dot{\xi}_N$ to take into account the effect of dissipation. The above equation is completely general and holds in any geometry, with $\boldsymbol{\psi}_N$ equal to the normal modes appropriate for the geometry in question. Here we are interested in a resonant sphere, so we must compute the right-hand side for the toroidal and spheroidal modes. For the toroidal modes $\boldsymbol{\psi}^T_{nlm}$, the integral vanishes for all l, and therefore they do not couple to GWs.[37] This is analogous to the fact that, in a cylindrical bar, the modes proportional to $\cos[\pi x(2n+2)/L]$ do not couple to GWs. They can therefore be used as a veto to distinguish spurious excitations due to noise from GWs.

We then turn our attention to the spheroidal modes. Writing them in the form (8.247) we have

$$\int d^3x\, (\boldsymbol{\psi}^S_{nlm})^*_i x_j = \int r dr d\Omega[A_{nl}(r)x_ix_jY^*_{lm} + B_{nl}(r)i\epsilon_{ipq}x_px_jL_qY^*_{lm}]\,. \tag{8.255}$$

[37] The proof is straightforward. Inserting the explicit form (8.250) of the toroidal modes, we are left with an integral of the type

$$\int d^3x\, f(r)x_j(iL_iY)^*\,,$$

where $f(r) = j_l(k^T_{nl}r)$, $Y \equiv Y_{lm}$ and $L_i = -i\epsilon_{ipq}x_p\partial_q$. We integrate ∂_q by parts, obtaining

$$\int d^3x\, f(r)x_j\epsilon_{ipq}x_p\partial_qY^*$$
$$= \int d^2S\, \hat{x}_q f(r)x_j\epsilon_{ipq}x_pY^*$$
$$-\epsilon_{ipq}\int d^3x\, Y^*x_p\partial_q\,[f(r)x_j]\,,$$

where d^2S is the surface element of the boundary, $\hat{x}_q = x_q/r$ is its normal, and we used $\epsilon_{ipq}\partial_qx_p = \epsilon_{ipq}\delta_{pq} = 0$. The first integral vanishes because $\epsilon_{ipq}x_p\hat{x}_q = 0$. In the second integral we use $\partial_q\,[f(r)x_j] = f'(r)\hat{x}_qx_j + f(r)\delta_{jq}$. The term $f'(r)\hat{x}_qx_j$ vanishes after contraction with $\epsilon_{ipq}x_p$, so we finally get

$$\int d^3x\, f(r)x_j(iL_iY)^*$$
$$= \epsilon_{ijk}\int d^3x\, f(r)x_kY^*. \tag{8.254}$$

The result is therefore antisymmetric in (i, j). In eq. (8.253) this quantity is contracted with h_{ij}, which is symmetric in (i, j), so the right-hand side of eq. (8.253) vanishes.

It is easy to see that the angular integral is non-vanishing only if $l = 0$ or $l = 2$. In fact, the symmetric and traceless tensor $x_i x_j - (1/3)\delta_{ij} r^2$ is a pure spin-2 tensor and therefore, expanding it in spherical harmonics, it contains only the harmonics with $l = 2$, i.e.

$$x_i x_j = \frac{1}{3}\delta_{ij} r^2 + r^2 \sum_{m'=-2}^{2} c_{ij}^{m'} Y_{2m'} \,, \tag{8.256}$$

where $c_{ij}^{m'}$ are coefficients, whose explicit form we do not need here (but we already found them in eq. (3.221)). Since the spherical harmonics are orthogonal, when we integrate the term proportional to $A_{nl}(r)$ over $d\Omega$ we find that $\delta_{ij} Y_{lm}^* \sim \delta_{ij} Y_{00} Y_{lm}^*$ gives a non-zero contribution only if $l = 0$, while $Y_{2m'} Y_{lm}^*$ gives a non-zero contribution only if $l = 2$. As for the term proportional to B_{nl}, recall from elementary quantum mechanics that the angular momentum operator L_p, acting on the spherical harmonics Y_{lm}, gives a combination of spherical harmonics with the same value of l. Therefore, $x_p x_j L_q Y_{lm}^*$ has a non-vanishing integral over the solid angle only if $l = 2$ (when $l = 0$ the term proportional to B_{nl} is absent from the spheroidal modes, see eq. (8.249)).

In general relativity h_{ij} is traceless and symmetric. Then, when in eq. (8.253) we perform the contraction with $\ddot{h}_{ij}$, the terms with $l = 0$ vanish since they are proportional to $A_{n0}(r)\delta_{ij}$. In conclusion, within the framework of general relativity, *GWs excite only the spheroidal modes with* $l = 2$.[38]

We can now compute the right-hand side of eq. (8.253), restricting to $l = 2$. It is convenient to write h_{ij} in terms of its spherical components h_m, with $m = -2, \ldots, 2$, introduced in Section 3.5.2. The h_m are defined as in eq. (3.222)

$$h_{ij}(t) = \sum_{m=-2}^{2} h_m(t) \mathcal{Y}_{ij}^{2m} \,, \tag{8.257}$$

where the five tensors $\mathcal{Y}_{ij}^{2m}$, with $m = -2, \ldots, 2$, are a basis in the space of the tensors traceless and symmetric with respect to the two indices (i, j), and are given explicitly in eq. (3.218). We insert this into eq. (8.253) and we compute explicitly the integral when $l = 2$. The result is

$$\frac{1}{2V} \ddot{h}_{ij} \int d^3x \, (\psi_{n2m}^S)_i^* x_j = \frac{1}{2} R \chi_n \ddot{h}_m \,, \tag{8.258}$$

where the coefficients χ_n are given by

$$\chi_n = \frac{3}{4\pi} \int_0^1 du \, u^3 \left[A_{n2}(\kappa_{n2} u) + 3 \, B_{n2}(\kappa_{n2} u) \right] \,, \tag{8.259}$$

and $\kappa_{nl} \equiv k_{nl}^S R$ is independent of R (the values for $l = 2$ and $n = 1, \ldots, 4$ are given in Table 8.1). The numerical values of χ_n for $n = 1, \ldots, 4$ and $\lambda/(2\mu) = 1.05$ are given in Table 8.3. Therefore eq. (8.253) becomes

$$\boxed{\ddot{\xi}_{nm} + \gamma_n \dot{\xi}_{nm} + \omega_n^2 \xi_{nm} = \frac{1}{2} R \chi_n \ddot{h}_m \,,} \tag{8.260}$$

[38] Some of the best motivated extensions of general relativity contain also gravitationally interacting scalar fields. In this case the trace of h_{ij} does not vanish (it is in fact expressed in terms of these scalar fields), and now the monopole mode $l = 0$ of the sphere can be excited. We understand from this a remarkable and unique property of a spherical resonant-mass detector: it can tell the spin content of the field that excites it, since the spin of the field matches exactly the value of l of the multipole modes that it excites.

where, for notational simplicity, we denoted ξ_{n2m}^S simply as ξ_{nm} and ω_{n2}^S as ω_n. Equation (8.260) shows another remarkable feature of a resonant sphere: the modes ξ_{nm} are sensitive only to the component h_m of the GW with the same m. Therefore, from the five quadrupolar modes ξ_{nm}, at n given, we can reconstruct the full matrix $h_{ij}(\omega)$, at the frequency $\omega = \omega_n$. This is different from what happens in resonant bars and, as we will see, in interferometers, where there is only a single output, of the form $h_+ F_+ + h_\times F_\times$, where $F_{+,\times}$ are functions that depend on the direction of the arrival of the GW (which is a priori unknown). The output of a sphere contains much more information, as we will see in detail in Section 8.4.2.

Comparing eq. (8.260) with eq. (8.3) we see that the quadrupolar modes ξ_{nm} of a sphere are formally equivalent to an oscillator with effective length $l_{\rm eff} = R\chi_n$ while, from the normalization condition (8.245), it follows that the effective mass of the modes is equal to mass M of the sphere.[39] Comparing with the results obtained for the fundamental mode of the cylinder of mass $M_{\rm cyl}$ and length L, we see that all results that we obtained for the fundamental mode of a cylindrical bar can be immediately applied to the spheroidal modes with $l = 2$ and n generic of a sphere of mass $M_{\rm sph}$, simply performing the replacements $(1/2)M_{\rm cyl} \to M_{\rm sph}$ and $(4/\pi^2)L \to \chi_n R$, and taking into account that the mode ξ_{nm} is driven by h_m rather than by h_{xx}.

We can then obtain the cross-section of the sphere for absorption of GWs, simply repeating the computations performed in Section 8.1.3. The result is

$$\boxed{\Sigma_n = F_n \frac{GM}{c} \left(\frac{v_s}{c}\right)^2 \,,} \tag{8.261}$$

with

$$F_n = \frac{8\pi^2}{15} \frac{\chi_n^2}{1 + \sigma_P} (R k_{n2}^S)^2 \,. \tag{8.262}$$

The numerical values of χ_n and F_n for $n = 1, \ldots, 4$ and $\lambda/(2\mu) = 1.05$ are given in Table 8.3. We see here another important advantage of a spherical resonant-mass detector, over a cylinder. A cylinder of length L and a sphere of radius R searching for GWs at the same frequency ω must have $L \simeq 2R$, as we see comparing eq. (8.14) with eq. (8.241) which, for a material such as aluminum, gives for $l = 2$ and $n = 1$ (the fundamental quadrupolar mode) $\omega \simeq 1.62 v_s/R$. However, a sphere with diameter L is much more massive than a thin cylinder of length L of the same material, and therefore its cross-section for GW absorption is much higher. Furthermore, for the sphere the sensitivity is isotropic, while for the bar we assumed a wave coming from the optimal direction. Averaging over all possible directions the bar cross-section is further reduced by a factor 4/15, see eq. (8.67).

[39] By definition of normal modes, the ξ_N are oscillators with frequencies ω_N, so the energy associated to ξ_N is proportional to $\dot{\xi}_N^2 + \omega_N^2 \xi_N^2$. The overall coefficient is found observing that the kinetic energy of an oscillation $\mathbf{u}(\mathbf{x}, t) = \xi_N(t) \boldsymbol{\psi}_N(\mathbf{x})$ is given by

$$\begin{aligned} &\frac{1}{2} \int dm \, |\dot{\mathbf{u}}|^2 \\ &= \frac{1}{2} \dot{\xi}_N^2 \int d^3x \, \rho(\mathbf{x}) |\boldsymbol{\psi}_N|^2 \\ &= \frac{1}{2} M \dot{\xi}_N^2 \,, \end{aligned}$$

where in the last line we used the normalization condition (8.245). Therefore the effective mass of the modes ξ_{nm} is equal to the mass M of the sphere.

Table 8.3 The values of χ_n and of F_n, for $n = 1, \ldots, 4$, setting $\lambda/(2\mu) = 1.05$.

n	χ_n	F_n
1	-0.328	2.996
2	-0.105	1.141
3	0.020	0.116
4	0.007	0.026

8.4.2 Spheres as multi-mode detectors

One of the most interesting features of a spherical resonant mass is that it is a multi-mode detector. A resonant cylinder is a single-mode detector because, at each resonant frequency ω_n, there is only one longitudinal mode. The output of a resonant cylinder is therefore a single quantity, the component of h_{ij} along the bar axis, say h_{xx}. This is related to the components h_+ and $h_\times$ of the GW and to the direction of arrival of the wave by $h_{xx} = h_+ F_+(\theta,\phi) + h_\times F_\times(\theta,\phi)$, where $F_{+,\times}(\theta,\phi)$ are the pattern functions of the bar. From this single output we cannot disentangle the information on the GW amplitude from that on the source direction. The same signal could be induced by a GW with a smaller amplitude but well oriented with respect to the bar, i.e. impinging transversally on it, or by a GW arriving from a less optimal direction, but with a higher amplitude. Even less can be said as to how this energy is shared between the two polarizations.

Therefore, if we detect a signal in a single cylindrical bar, in the absence of an optical counterpart the best one can do is to guess that the wave came from a more-or-less optimal direction and to guess that $h_+ \sim h_\times$, and under these assumptions one can estimate the energy flux carried by the wave. Almost nothing can be said about the source location, except that it cannot be too close to the bar's blind direction, which is its longitudinal axis. As we will see in later chapters, the situation is similar for a single interferometer, and to improve it substantially, with bars or interferometers, it is necessary to detect the signal simultaneously in different detectors.

A sphere is completely different from this point of view. At each resonance frequency ω_n, corresponding to an $l = 2$ spheroidal mode, it has five degenerate modes coupled to the GWs, and therefore a sphere has five independent outputs. As we have seen in eq. (8.260), each of the five modes ξ_{nm} (with n given and $m = -2,\dots,2$) is driven only by the spherical component $\tilde h_m(\omega_n)$ of the GW which has the same value of m. Therefore, monitoring the five ξ_{nm} we obtain the five quantities $\tilde h_m(\omega_n)$ and, using eq. (8.257), we can reconstruct the full matrix $\tilde h_{ij}$ at the resonance frequency or, more precisely, in a bandwidth centered around ω_n.

The full matrix $\tilde h_{ij}$ contains all the information on the arrival direction and on the amplitude of the two polarizations. In particular, if the excitation of the detector is really due to a GW, rather than to noise, it must be possible to rotate the axes of our reference frame so that the new z axis coincides with the propagation direction of the wave. In other words, once we measure the quantities h_m and we construct h_{ij} as in eq. (8.257), it must exist a rotation $\mathcal{R}$ such that

$$\mathcal{R}_{ik}\mathcal{R}_{jl}h_{kl} = \begin{pmatrix} h_+ & h_\times & 0 \\ h_\times & -h_+ & 0 \\ 0 & 0 & 0 \end{pmatrix}_{ij} . \tag{8.263}$$

Then the propagation direction $\hat{\mathbf{n}}$ of the GW is obtained applying this

rotation to the original z axis, i.e. $n_i = \mathcal{R}_{ij}\hat z_j = \mathcal{R}_{i3}$. Given the original matrix h_{ij}, the determination of the incoming direction (in the absence of noise) is therefore a straightforward algebraic problem, whose solution is

$$\tan\varphi \equiv n_y/n_x = \frac{h_{22}h_{13} - h_{12}h_{23}}{h_{12}h_{13} - h_{11}h_{23}} , \tag{8.264}$$

$$\tan\theta \equiv \frac{(n_x^2+n_y^2)^{1/2}}{n_z} = \frac{h_{13}}{h_{12}\cos\varphi - h_{11}\sin\varphi} . \tag{8.265}$$

We have therefore reconstructed the arrival direction, up to a sign ambiguity: we cannot distinguish a wave coming from the direction $\hat{\mathbf{n}}$ from a wave coming from $-\hat{\mathbf{n}}$, since if (θ,φ) satisfy eqs. (8.264) and (8.265) then also $(\pi-\theta,\pi+\varphi)$ satisfy it. (This ambiguity could be fixed measuring the time delay between two detectors.) We have therefore determined the arrival direction and we can now read the two separate amplitudes h_+ and $h_\times$ from eq. (8.263).[40]

At this stage we have used five outputs to determine four quantities: the two amplitudes $h_+, h_\times$ (or, equivalently, the amplitude $h = (h_+^2 + h_\times^2)^{1/2}$ and the polarization angle Ψ defined by $h = h_+\cos 2\Psi + h_\times \sin 2\Psi$), and the two angles θ,ϕ that give the unit vector $\hat{\mathbf{n}}$. We still have one unused information. This is a veto that distinguishes GWs from spurious events due to noise. In fact, given five arbitrary numbers h_m, the matrix $\sum_m h_m \mathcal{Y}^m_{ij}$ is by definition traceless and symmetric, because the $\mathcal{Y}^m_{ij}$ are traceless and symmetric, but this just means that, with an appropriate rotation, we can bring it to the form

$$\begin{pmatrix} a & d & 0 \\ d & b & 0 \\ 0 & 0 & c \end{pmatrix}_{ij} , \tag{8.266}$$

with $a+b+c=0$. That is, we can choose two Euler angles associated to a rotation to set to zero the (1,3) and (2,3) elements of the matrix (and of course at this point we can also set $d=0$ with a rotation around the new z axis). The fact that, after performing such a rotation, we automatically find $c=0$ and therefore $a=-b$ is instead a specific property of GWs, due to their transverse nature. In conclusion, the five quadrupolar modes of the sphere allow us to determine the source direction $\hat{\mathbf{n}}$ (up to a sign ambiguity $\hat{\mathbf{n}} \to -\hat{\mathbf{n}}$), the two separate amplitudes h_+ and $h_\times$, and to have a veto that discriminates GWs from noise.

Other vetoes emerge naturally in a resonant sphere. For instance, from Tables 8.1 and 8.2 we see that the toroidal mode with $l=2, n=1$ is quite close, in frequency, to the spheroidal mode with $l=2, n=1$. Since the former is not coupled to GWs while the latter is the main mode that is monitored for GW detection, an excitation of the latter when the former is not excited would give further confidence on the GW origin of the signal.[41]

We have seen above that, in the ideal case in which the signal is given uniquely by the GWs, and the noise is negligible, a sphere is able to locate *exactly* the direction of the source, contrary to a single bar or

[40] Of course, once we find a rotation that brings h_{ij} to the form (8.263), any further rotation around the new z axis still leaves h_{ij} in this form. This further rotation just amounts to a redefinition of the axes with respect to which the two polarizations are defined, and mixes h_+ and $h_\times$ as in eq. (2.194). In particular, it can be chosen so that $h_\times$ is set to zero and h_{ij} becomes diagonal, $h_{ij} = \mathrm{diag}\,(h_+, -h_+, 0)$.

[41] Toroidal modes have no radial displacement, so to detect them we need transducers coupled to the transverse oscillations of the surface.

a single interferometer that, even in the ideal noiseless limit, have an angular resolution of order 4π. Of course, in a real situation noise is present, and the angular resolution of the sphere depends on the signal-to-noise ratio. We denote by θ_0 and ϕ_0 the actual angles which give the direction of propagation of the wave and by θ_c and ϕ_c the angles computed from the five outputs of a noisy resonant sphere. We introduce the notation $\Delta\theta = \theta_c - \theta_0$ and $\Delta\phi = \phi_c - \phi_0$. A useful indicator of the angular resolution is

$$\Delta\Omega \equiv \pi \left[(\Delta\theta)^2 + \sin^2\theta_0 (\Delta\phi)^2 \right] , \tag{8.267}$$

which is the area of a circle on the unit sphere, centered on the actual source location, and with radius $\delta\hat{\mathbf{n}} = \hat{\mathbf{n}}_c - \hat{\mathbf{n}}_0$, where $\hat{\mathbf{n}}_0$ is the unit vector of the actual propagation direction of the GW and $\hat{\mathbf{n}}_c$ is the direction computed from the noisy outputs. Then it can be shown (Zhou and Michelson 1995, Stevenson 1997) that, if we denote by SNR the signal-to-noise ratio in energy, in the limit of large SNR the angular resolution is given by

$$(\Delta\theta)^2 = \sin^2\theta_0 (\Delta\phi)^2 = \frac{1}{\mathrm{SNR}} , \tag{8.268}$$

and therefore

$$\boxed{\Delta\Omega = \frac{2\pi}{\mathrm{SNR}} .} \tag{8.269}$$

A spherical resonant mass detector, MiniGRAIL, has been developed at Leiden University, in the Netherlands, and is in its commissioning phase. It is a sphere of 68 cm of diameter and a mass $M \simeq 1.3$ ton, shown in Fig. 8.20. At 4 K its spheroidal quadrupolar modes are at $f \simeq 2980$ Hz. The material is an alloy CuAl6%, chosen because of its high quality factor ($Q \sim 10^7$ at low T), high sound velocity ($v_s \simeq 4100$ m/s) and a sufficient thermal conductivity, which already allowed to cool it below 100 mK. The ultimate goal is to operate it at a thermodynamical temperature $T \simeq 20$ mK. The expected bandwidth should be of order 230 Hz, and possibly higher. The quadrupole modes are monitored using various transducers, coupled to double-stage SQUID amplifiers. The optimal choice is to have six transducers in the so-called TIGA configuration, see the Further Reading section. The target is to reach a temperature $T = 20$ mK, and a strain sensitivity $S_h^{1/2}$ of order $10^{-22} - 10^{-23}\,\mathrm{Hz}^{-1/2}$. The present sensitivity is shown in Fig. 8.21.

Since its size is relatively small, MiniGRAIL explores high frequencies, in the 3 kHz region. As we will discuss in Vol. 2, this could still be an interesting region for astrophysical signals from compact objects.

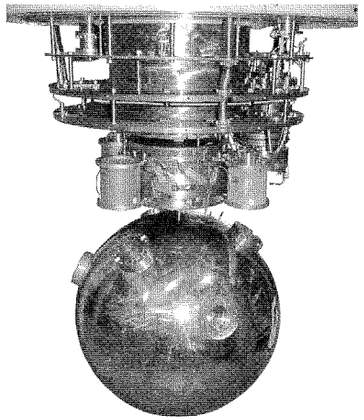

Fig. 8.20 The MiniGRAIL resonant sphere. A few resonant transducers are also visible.

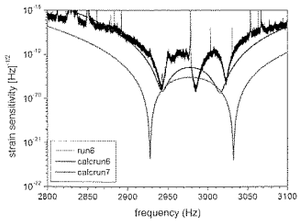

Fig. 8.21 The strain sensitivity of MiniGRAIL (as of Jan 2005) compared to the prediction of a simplified two-mode model, cooling the detector to a temperature $T = 5$ K. The lowest curve is the sensitivity expected cooling at $T = 80$ mK. The final goal is to reach $T = 20$ mK.

Further reading

- A historical account of GW research can be found in Thorne (1987). For overviews of resonant bars see e.g. Thorne (1987), Coccia (1997), Ju, Blair and Zhao (2000) and Bassan (2002).
- Computations of the sensitivity of resonant bars can be found in Pallottino and Pizzella (1981, 1984, 1991), Michelson and Taber (1981,1984), and Price (1987). It is interesting to observe that the role of the amplifier noise was first pointed out by two distinguished theorists, Gibbons and Hawking (1971).
- Resonant transducers have been proposed by Paik (1976). For detailed reviews on passive transducers see Richard and Folkner (1991). Parametric transducer are discussed in Veitch (1991) and in Ju, Blair and Zhao (2000). The dual scheme is proposed in Cerdonio *et al.* (2001) and Briant *et al.* (2003). See also the review Cerdonio (2003).
- For back-action and the quantum limit in resonant bars see Giffard (1976). Quantum nondemolition measurements are discussed in detail in Caves, Thorne, Drever, Sandberg and Zimmermann (1980) and in Braginsky and Kalili (1992).
- Analysis of the coincidences between the five resonant bars ALLEGRO, AURIGA, EXPLORER, NAUTILUS and NIOBE, and the relative upper limit on GW bursts, can be found in Allen *et al.* [IGEC] (2000) and Astone *et al.* [IGEC] (2003a). Searches for periodic GWs are reported in Astone *et al.* [ROG] (2002).
- Descriptions of the detectors can be found in Astone *et al.* (1997b) for NAUTILUS, Astone *et al.* (2003b) for EXPLORER, Blair *et al.* (1995) for NIOBE, Mauceli *et al.* (1996) for ALLEGRO, M. Cerdonio *et al.* (1997) and J.-P. Zendri *et al.* (2002) for AURIGA.

  For information on the resonant bar experiments see the links:

  http://sam.phys.lsu.edu
  http://www.auriga.lnl.infn.it
  http://www.roma1.infn.it/rog/explorer
  http://www.lnf.infn.it/esperimenti/rog/nautilus

  Coordination among the various GW experiments (both resonant masses and interferometers) is provided by the Gravitational Wave International Committee (GWIC), see the link http://gwic.gravity.psu.edu
- The advantages of a resonant sphere in terms of cross-section and its multi-mode capability were already realized in the 1970s, see Forward (1971), Ashby and Dreitlein (1975) and Wagoner and Paik (1977). Detailed discussion of spherical detectors can be found in Zhou and Michelson (1995), Lobo (1995) and Coccia, Lobo and Ortega (1995). Hollow spheres are studied in Coccia, Fafone, Frossati, Lobo, and Ortega (1998) and Lobo (2002). The multi-frequency capability of the sphere and the possibility of reconstruction of the chirp mass and orbital parameters of a coalescing binary with a single sphere is discussed in Coccia and Fafone (1996) and Spallicci, Frossati and Krolak (1997). The response of a resonant sphere to GWs in extensions of general relativity is discussed in Bianchi, Coccia, Colacino, Fafone and Fucito (1996) and, for scalar fields, in Bianchi, Brunetti, Coccia, Fucito and Lobo (1998) and Maggiore and Nicolis (2000).
- A particularly useful configuration of transducers for a spherical detector, the TIGA configuration, was proposed and investigated experimentally in Johnson and Merkowitz (1993) and Merkowitz and Johnson (1995, 1997). See also the PhD thesis of Merkowitz (1995). Another configuration requiring only five transducers, but with four of them sensitive to transverse displacements, is proposed in Zhou and Michelson (1995). Detailed discussion of sensitivity and optimal filtering in the presence of multiple transducers is given in Stevenson (1997).
- For MiniGRAIL, see de Waard, Gottardi, van Houwelingen, Schumack, and Frossati (2003), and the PhD theses of de Waard (2003) and of Gottardi (2004). Updated information can be found at http://www.minigrail.nl. Another spherical resonant-mass under development is the "Mario Schenberg" detector of the Brazilian GRAVITON project, see Aguiar (2004).